Description of the PlankTOM10 equations

April 17, 2014

1 Introduction

This Appendix presents a full description of the PlankTOM10 model, a global marine biogeochemical model based on the representation of ten Plankton Functional Types (PFTs), including six phytoplankton (pPFTs), three zooplankton (zPFTs) and bacteria. PlankTOM10 also represents the full cycles of C, O_2, P and Si and simplified cycles for Fe and N. It currently comprises of 39 biogeochemical tracers (Table 1).

1.0.1 Notation

In the following sections, we will show the equations governing tracer and food-web dynamics. These equations are mostly semi-empirical, and have been developed and tested using a multitude of laboratory and field data. As long as not otherwise indicated, both tracers and their respective concentrations will be designated by capital letters, with

- P_i: concentration of pPFT$_i$ with $i \in \{1, 6\}$,
- Z_j: concentration of zPFT$_j$, with $j \in \{1, 3\}$,
- F_k: concentration of food k; where F_k includes phytoplankton and other food sources
- PRO: proto-zooplankton concentration,
- MES: meso-zooplankton concentration,
- MAC: macro-zooplankton concentration,
- PO_4: concentration of phosphate,
- DIN: concentration of dissolved, inorganic nitrogen,
- Fe: iron concentration, and
- Si: silicate concentration.

All concentrations are calculated in $\frac{mol}{L}$ except for chlorophyll whic is in $\frac{gCHL}{L}$.

Tables and an index are provided which link the mathematical symbols with the variable names used in the Fortran code.

Where subscript j includes pico-heterotrophs in additon to the three zoo-plankton types this is stated explicitly.

The ten plankton functional types and the tracers are shown in Figure 1.Figures of this type showing the processes governing the evolution of the PFTs and tracers are included in the following sections.

Table 1: List of biogeochemical Tracers in PlankTOM10

Abbreviation	**Description**	**Units**
ALK	alkalinity	eq L^{-1}
BAC	pico-heterotrophs	mol L^{-1}
BFE	Fe in large POM	mol L^{-1}
BSI	biogenic particulate silica	mol L^{-1}
CAL	sinking $CaCO_3$	mol L^{-1}
CCH	chlorophyll in calcifiers	g L^{-1}
CFE	Fe in calcifiers	mol L^{-1}
COC	calcifying phytoplankton	mol L^{-1}
DCH	chlorophyll in silicifiers	g L^{-1}
DFE	Fe in silicifiers	mol L^{-1}
DIA	silicifying phytoplankton	mol L^{-1}
DIN	dissolved inorganic nitrogen	mol L^{-1}
DIC	dissolved inorganic carbon	mol L^{-1}
DOC	dissolved organic carbon	mol L^{-1}
DSI	sinking particulate silica	mol L^{-1}
FER	dissolved iron	mol L^{-1}
FCH	chlorophyll in N_2 fixers	g L^{-1}
FFE	Fe in N_2 fixers	mol L^{-1}
FIX	N_2 fixing phytoplankton	mol L^{-1}
GOC	large particulate organic carbon	mol L^{-1}
HCH	chlorophyll in DMSP producers	mol L^{-1}
HFE	Fe in DMSP producers	mol L^{-1}
PIC	pico-phytoplankton	mol L^{-1}
MES	meso-zooplankton	mol L^{-1}
MIX	mixed phytoplankton	mol L^{-1}
NCH	chlorophyll in mixed phytoplankton	g L^{-1}
NFE	Fe in mixed phytoplankton	mol L^{-1}
OXY	dissolved oxygen	mol L^{-1}
PCH	chlorophyll in pico-phytoplankton	g L^{-1}
PFE	Fe in pico-phytoplankton	mol L^{-1}
PIC	pico-phytoplankton	mol L^{-1}
PHA	DMSp producing phytoplankton	mol L^{-1}
PO4	generic macronutrient	mol C L^{-1}
POC	small particulate organic carbon	mol L^{-1}
PRO	proto-zooplankton	mol L^{-1}
SFE	Fe in small POM	mol L^{-1}
SIL	dissolved SiO_3	mol L^{-1}

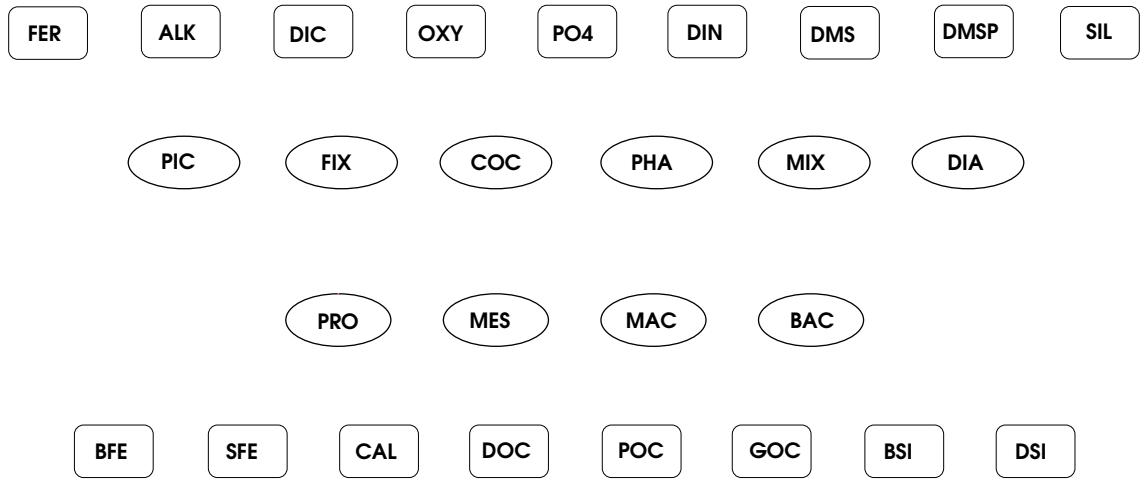

Figure 1: The constituents of PlankTOM10; PFTs are shown as ellipses and tracers as rounded rectangles.There are also tracers for the chlorophyll and iron content of the individual pPFTs but these have been omitted from the figures for clarity.

1.0.2 Tracer Transport

The temporal evolution of all passive tracers T is governed by the balance between its local sources and sinks ('Sources-Minus-Sinks' (SMS), biogeochemical part) and by the physical transport processes (advection and diffusion), hence

$$\frac{dT}{dt} = \nabla \cdot (\vec{u}T) + \nabla \cdot (\vec{K}\nabla T) + SMS, \tag{1}$$

where $\vec{K}$ is the 3-dimensional tracer diffusion coefficient and $\vec{u}$ is the fluid velocity, calculated in the physical model. To ensure numerical stability, the sinks processes in SMS are set to zero then the concentration of passive tracers fall below a set threshold (1.e-10).

2 Autotrophic PFTs

2.1 Phytoplankton Biomass - PIC, FIX, COC, PHA, MIX, DIA

The processes governing evolution of phytoplankton biomass for each P_i is shown in Figure 2. Evolution in terms of carbon is described in this section; chlorophyll (Section 2.2) and iron in phytoplankton (Section 6.1.1) are modelled silimarly. Growth of phytoplankton modifies dissolved organic carbon (Section 4.1), silica (Section 6.2), calcium carbonate (Section 5.1), phosphate, dissolved inorganic nitrogen (Section 6.3), alkalinity (Section 5.3) and oxygen (Section 6.4) in the ocean. The temporal evolution of phytoplankton biomass is given in the equation below:

$$\begin{aligned} \frac{\partial P_i}{\partial t} &= \underbrace{\mu^{P_i} P_i}_{production} - \underbrace{\mu_0^{P_i} \delta_{P_i} b_{P_i}^T P_i}_{loss} \\ &- \underbrace{\sum_j g_{P_i}^{Z_j} Z_j P_i}_{grazing} \end{aligned} \tag{2}$$

$g_{P_i}^{Z_j} * Z_j * P_i$ describes the amount of biomass lost in grazing by the zPFT $Z_j, j \in \{1, 3\}$ as described in Section 3. In the present configuration of the model all available phytoplankton are grazed so there is no mortality term.

μ_P is the phytoplankton growth rate and is a function of temperature, light and nutrient availability:

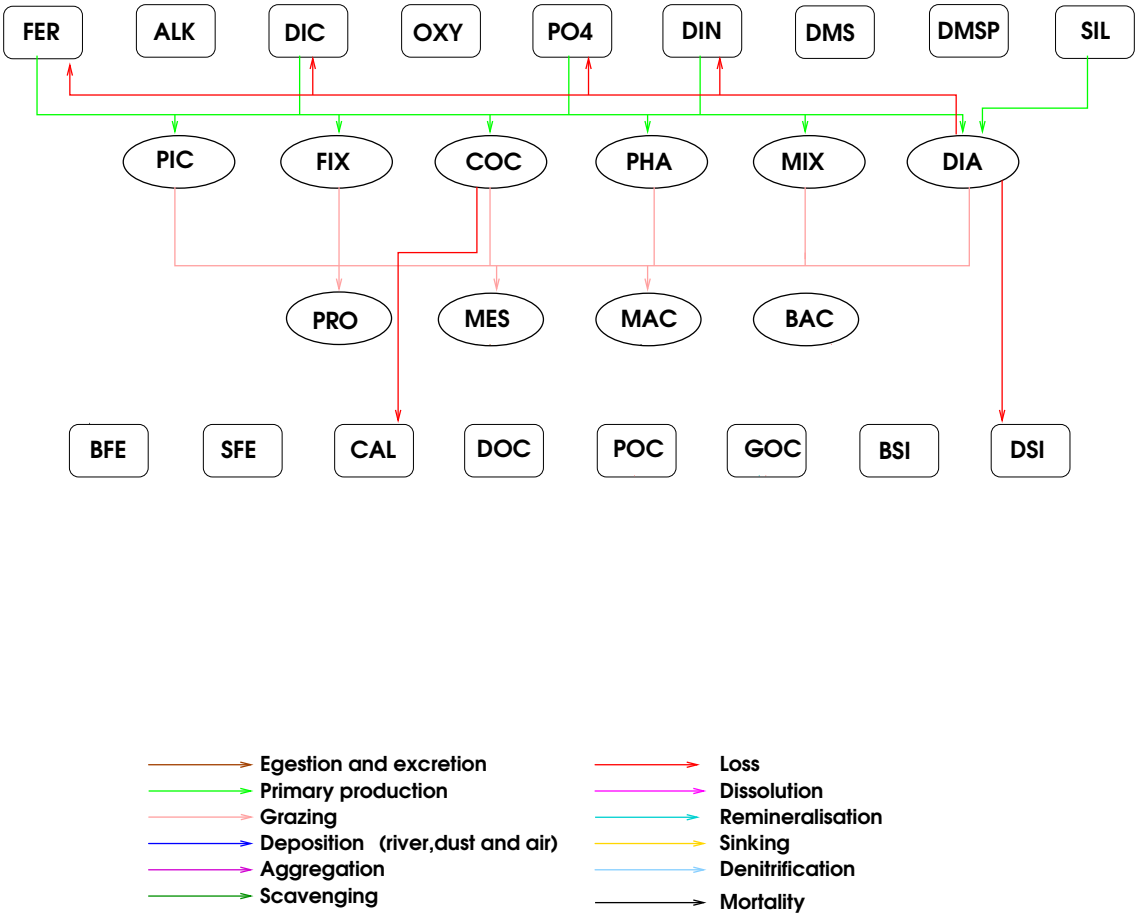

Figure 2: The processes governing the development of the phytoplankton.

$$\begin{aligned} \mu^{P_i} &= \mu_0^{P_i} * f(T) * f(PAR) * f(nut) \\ &= \mu_0^{P_i} * (1 + \delta^{P_i}) * b_{P_i}^T * L_{light}^{P_i} * L_{lim}^{P_i} \end{aligned} \tag{3}$$

where $\mu_0^{P_i}$ is the maximum growth rate at 0° C, b_{P_i} is the temperature dependence of the growth rate and T is the temperature. For coccolithophorids the growth rate below 10° is reduced to $(.2 + .8 * \frac{T}{10.}) * b_{coc}^T$.

The radiation available for photosynthesis is dependent on the wavelength and the depth:

$$\begin{aligned} PAR(z + \Delta z) &= .215 * Q_{sr} * e^{-\left(\sum_i x_g + CHL^{P_i} * y_g^{P_i}\right)\Delta z} \\ &+ .215 * Q_{sr} * e^{-\left(\sum_i x_r + CHL^{P_i} * y_r^{P_i}\right)\Delta z}. \end{aligned} \tag{4}$$

where the fraction of available solar radiation Q_{sr} which is in the photosynthetically active wavelength range has been divided between the blue/green and red wavelengths, x_g, x_r are the extinction coefficients of pure water for blue/green and red wavelengths and $y_g^{P_i}$, $Y_r^{P_i}$ are the extinction coefficients of chlorophyll. If

$$perfrm = \alpha^{P_i} * \frac{CHL^{P_i}}{P_i} 4.6 * PAR(z) \tag{5}$$

and

$$pctnut = \mu_0^{P_i} * (1 + \delta^{P_i}) * b_{P_i}^T * L_{lim}^{P_i} \tag{6}$$

then

$$L_{light} = 1 - e^{-\frac{perfrm}{pctnut}} \tag{7}$$

The nutrient limitation ($L_{lim}^{P_i}$) determines the limitation of the growth rate due to the availability of nutrients. It is assumed that nutrient limitation follows Michaelis-Menten kinetics and that growth is determined by the least available nutrient. Hence, for phytoplankton other than silicifiers and nitrogen fixers:

$$L_{lim}^{P_i} = \min\left(\frac{PO_4}{PO_4 + K_{PO_4}^{P_i}}, \frac{\frac{Fe_{P_i}}{P_i} - Fe_{P_i}^{min}}{Fe_{P_i}^{opt} - Fe_{P_i}^{min}}, \frac{DIN}{DIN + K_{DIN}^{P_i}}\right) \tag{8}$$

for silicifiers:

$$L_{lim}^{DIA} = \min\left(\frac{PO_4}{PO_4 + K_{PO_4}^{DIA}}, \frac{\frac{Fe_{DIA}}{DIA} - Fe_{DIA}^{min}}{Fe_{DIA}^{opt} - Fe_{DIA}^{min}}, \frac{DIN}{DIN + K_{DIN}^{DIA}}, \frac{Si}{Si + K_{Si}^{DIA}}\right). \tag{9}$$

and for nitrogen fixers:

$$L_{lim}^{FIX} = \min\left(\frac{PO_4}{PO_4 + K_{PO_4}^{FIX}}, \frac{\frac{Fe_{FIX}}{FIX} - Fe_{FIX}^{min}}{Fe_{FIX}^{opt} - Fe_{FIX}^{min}}, \frac{DIN}{DIN + K_{DIN}^{FIX}} + R_{FIX}\left(1 - \frac{DIN}{DIN + K_{DIN}^{FIX}}\right)\right) \tag{10}$$

2.2 Primary Production, Photosynthesis and Chlorophyll - DCH, NCH, CCH, PCH, HCH, FCH

The chlorophyll content of each phytoplankton type (DCH for silicifiers, NCH for mixed-phytoplankton, CCH for calcifiers and PCH for picophytoplankton, HCH for DMSp and FCH for N_2-fixers) is modelled. Chlorophyll evolves in a very similar fashion to phytoplanktonic biomass (see equation 3), as sources and sinks of chlorophyll are of phytoplanktonic origin. The iron-light colimitation model is a dynamical photosynthesis model in which the rate of photosynthesis both controls cellular iron and chlorophyll synthesis and is controlled by their quota (Buitenhuis and Geider, 2010).

Table 2: List of Parameters and variables used to compute the evolution of phytoplankton

Term	Variable	Description	Defined in
δ_{P_i}	rn_resphy	respiration as fraction of growth	*sms.F90*
$\mu_0^{P_i}$	rn_mumpft	maximum growth rate at 0°C	*namelist.trc.sms*
μ^{P_i}	prophy	productivity of phytoplankton P_i	*bgcpro.F90*
b_{P_i}	rn_mutpft	temperature dependence of growth rate	*namelist.trc.sms*
α^{P_i}	rn_alpphy	initial slope of photosynthesis vs light intensity curve	*namelist.trc.sms*
PAR	etot	Photosynthetcally active radiation	*bgcpro.F90*
Q_{sr}	qsr	surface solar radiation	*traqsr.F90*
x_g	rn_ekwgrn	absorption coefficient of water for blue-green light	*namelist.trc.sms*
x_r	rn_ekwred	absorption coefficient of water for red light	*namelist.trc.sms*
$y_g^{P_i}$	rn_kgrphy	light absorption in blue-green	*namelist.trc.sms*
$y_r^{P_i}$	rn_krdphy	light absorption coefficient for red	*namelist.trc.sms*
$perfrm$	perfrm	photosynthetic performance	*bgcpro.F90*
$pctnut$	pctnut	macronutrient and temperature defined growth rate	*bgcpro.F90*
L_{light}	xlim8	Light limitation for phytoplankton growth	*bgcpro.F90*
$Fe_{P_i}^{max}$	rn_qmaphy	Maximum Fe quota	*namelist.trc.sms*
$Fe_{P_i}^{min}$	rn_qmiphy	Minimum Fe quota	*namelist.trc.sms*
$Fe_{P_i}^{opt}$	rn_qopphy	Optimum Fe quota	*namelist.trc.sms*
$K_{DIN}^{P_i}$	rn_kmnphy	half-saturation coefficients for DIN	*namelist.trc.sms*
$K_{PO4}^{P_i}$	rn_kmpphy	half-saturation coefficients for $PO4$	*namelist.trc.sms*
K_{SIL}^{DIA}	rn_sildia	half-saturation coefficient for SIL in diatoms	*namelist.trc.sms*
$L_{lim}^{P_i}$	xlimpft	macronutrient limitation for phytoplankton growth	*bgcpro.F90*

$$\begin{aligned} \frac{\partial Chl^{P_i}}{\partial t} &= \underbrace{\rho_{Chl}^{P_i} L_{light} pctnut P_i}_{production} - \underbrace{\mu_0^{P_i} \delta_{P_i} b_{P_i}^T * Chl^{P_i}}_{loss} \\ &- \underbrace{\sum_j g_{P_i}^{Z_j} Z_j \frac{Chl_{P_i}}{P_i}}_{grazing}, \end{aligned} \tag{11}$$

where

$$\rho_{Chl}^{P_i} = \theta_{chl}^{P_i} * pctnut * \frac{L_{light}}{perfrm} \tag{12}$$

$\theta_{chl}^{P_i}$ is the maximum chlorpophyll to carbon ratio for phytoplankton P_i and $perfrm$ and $pctnut$ are defined in equations 5 and 6

Table 3: List of parameters and variables used to calculate the evolution of chlorophyll

Term	Variable	Description	Defined in
$\theta_{Chl}^{P_i}$	rn_thmphy	maximum CHL:C ratio	*namelist.trc.sms*
$\rho_{Chl}^{P_i}$	rhochl	regulation term of chlorophyll synthesis	*bgcpro.F90*

3 Heterotrophic PFT's

The temporal evolution of zooplankton and the pico-heterotrophs are shown in Figure 3.

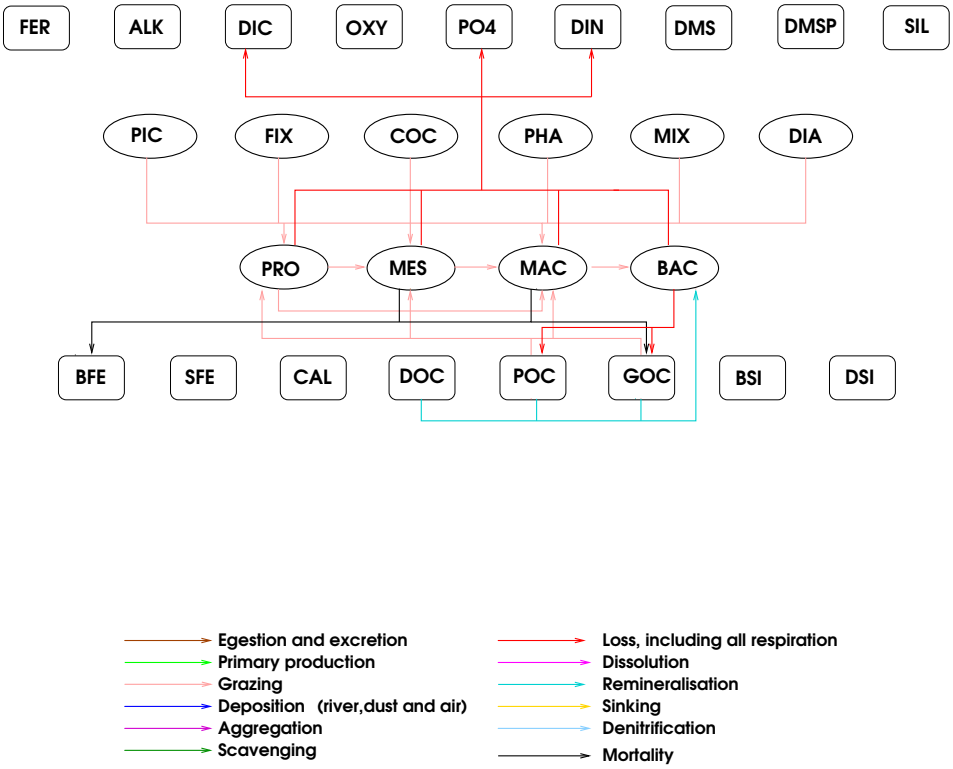

Figure 3: The processes governing the development of the zooplankton and pico-heterortrophs.

3.1 Zooplankton Biomass - PRO, MES and MAC

The temporal evolution of zooplankton concentrations Z_j in PlankTOM are described as follows (Buitenhuis et al., 2006):

$$\begin{aligned}\frac{\partial Z_j}{\partial t} &= \underbrace{\sum_k g_{F_k}^{Z_j} * F_k * MGE * Z_j}_{growth\ through\ grazing} - \underbrace{\sum_{k=j+1}^{3} g_{Z_j}^{Z_k} * Z_k * Z_j}_{loss\ through\ grazing} - \underbrace{R_{0^\circ}^{Z_j} * d_{Z_j}^{T} * Z_j}_{basal\ respiration} \\ &- \underbrace{m_{0^\circ}^{Z_j} * c_{Z_j}^{T} * \frac{Z_j}{K^{Z_j} + Z_j} * \sum_i P_i}_{mortality\ through\ predation}, \end{aligned} \tag{13}$$

where $g_{F_k}^{Z_j}$ is the grazing of zooplankton Z_j on food source F_k and MGE is the growth efficiency. $R_{0^\circ}^{Z_j}$ is the respiration rate at 0°C, d_{Z_j} is the temperature dependence of the respiration ($d^{10} = Q_{10}$).,$m_{0^\circ}^{Z_j}$ is the mortality rate at 0°C, c_{Z_j} is the temperature dependence of the mortality ($c^{10} = Q_{10}$). K^{Z_j} is the half saturation constant for mortality and is set to$20 * 10^{-6}$. The mortality term for meso- and macrozooplankton is due to predation by top predators for which the total protozooplankton and phytoplankton biomass is used as a proxy. In the presence of ice krill are protected from predation so the macrozooplankton mortality is reduced by a factor of .01.

Grazing $g_{F_k}^{Z_j}$, of zooplankton Z_j on food source F_k is dependent on the zooplankton preference, $p_{F_k}^{Z_j}$,

the concentration of the food source and the temperature.

$$g_{F_k}^{Z_j} = g_{max}^{Z_j}(T)\frac{p_{F_k}^{Z_j}}{K^{Z_j} + \sum_i p_{F_k}^{Z_j} F_k} \tag{14}$$

The food sources F for zooplankton are summarised in Table 4. For macro-zooplankton they are phytoplankton, meso-zooplankton, proto-zooplankton, pico-heterotrophs, small and large particulate organic matter. The food sources F for meso-zooplankton are phytoplankton, proto-zooplankton, pico-heterotrophs, small and large particulate organic matter. The food sources for proto-zooplankton are phytoplankton, pico-heterotrophs, small and large particulate organic matter.

Table 4: Food sources for zooplankton and pico-heterotrophs

Food	Macro-zooplankton	Meso-zooplankton	Proto-zooplankton	Pico-heterotrophs
Meso-zooplankton	*			
Proto-zooplankton	*	*		
Phytoplankton	*	*	*	
Pico-heterotrophs	*	*	*	
Large POM	*	*	*	*
Small POM	*	*	*	*
Dissolved OM				*

The temperature dependence of the grazing rate is:

$$g_{max}^{Z_j}(T) = g_{0^\circ}^{Z} b_{Z_j}^{T}, \tag{15}$$

where $g_{0^\circ}^{Z}$ is the maximum grazing rate at 0° C, b_{Z_j} is the temperature dependence of the grazing rate ($b^{10} = Q_{10}$), T is the local seawater temperature in °Celsius. In shallow water (<600m) in the summer months under ice coverage of between .1 and .3 macrozooplankton experience enhanced recruitment (Wiedenmann et al., 2009). This is included by increasing the growth rate by a factor r_{MAC} when these conditions apply.

The model growth efficiency MGE, a function of gross growth efficiency (GGE), describes the fraction of grazed food incorporated into zooplankton biomass and basal respiration normalised to all material ingested:

$$MGE_{Z_j} = MIN\left(1 - \xi^{Z_j}, GGE_{Z_j} + \frac{R_{0^\circ}^{Z_j} * d_{Z_j}^{T} * Z_j}{\sum_k g_{F_k}^{Z_j}}\right). \tag{16}$$

Equation 41 shows the possible reduction in MGE_{Z_j} when zooplankton graze on phytoplankton with a lower $\frac{Fe}{C}$ ratio than themselves.

3.2 Pico-heterotrophs

The temporal evolution of bacterial concentration is modelled in a similar way to zooplankton:

$$\begin{aligned}\frac{\partial BAC}{\partial t} = & \underbrace{\lambda_{OC}^{*}(T) BGE * BAC}_{growth\ through\ remineralisation} - \underbrace{R_{0^\circ}^{BAC} * d_{BAC}^{T} * BAC}_{respiration} \\ & - \underbrace{\sum_j g_{BAC}^{Z_j} * BAC * Z_j}_{grazing}\end{aligned} \tag{17}$$

where BGE is the bacterial growth efficiency. The food sources F_k for bacteria are DOC and small and large particulate organic carbon. Mineralisation rate $\lambda_{OC}^{*}(T)$ is dependent on the temperature and the available food:

Table 5: List of parameters and variables used to calculate the evolution of zooplankton

Term	Variable	Description	Defined in
$g_0^{Z_j}$	rn_gramic	maximum grazing rate at 0^o	*namelist.trc.sms*
	rn_grames	for proto-, meso-	*namelist.trc.sms*
	rn_gramac	and macrozooplankton	*namelist.trc.sms*
$g_{max}^{Z_j}$	graze	grazing rate for proto-	*bgclos.F90*
	graze2	meso- and	*bgclos.F90*
	graze3	macrozooplankton	*bgclos.F90*
b_{Z_j}	rn_mutpft	Temperature dependence of grazing	*namelist.trc.sms*
		for proto, meso- and	*namelist.trc.sms*
		macro-zooplankton	*namelist.trc.sms*
r_{MAC}	rn_icemac	enhanced recruitment factor under ice	*namelist.trc.sms*
p_F^Z	rn_gmibac	proto-zoo. grazing preference for bacteria	*namelist.trc.sms*
	rn_gmigoc	proto-zoo. grazing preference for GOC	*namelist.trc.sms*
	rn_gmipoc	proto-zoo. grazing preference for POC	*namelist.trc.sms*
	rn_gmiphy	proto-zoo. grazing preference for phyto.	*namelist.trc.sms*
	rn_gmebac	meso-zoo preference for bacteria	*namelist.trc.sms*
	rn_gmegoc	meso-zoo. grazing preference for GOC	*namelist.trc.sms*
	rn_gmepoc	meso-zoo. grazing preference for POC	*namelist.trc.sms*
	rn_gmemic	meso-zoo. grazing preference for proto-zoo.	*namelist.trc.sms*
	rn_gmephy	meso-zoo. grazing preferencefor phyto	*namelist.trc.sms*
	rn_gmabac	macro-zoo preference for bacteria	*namelist.trc.sms*
	rn_gmagoc	macro-zoo preference for GOC	*namelist.trc.sms*
	rn_gmames	macro-zoo preference for meso-zoo	*namelist.trc.sms*
	rn_gmamic	macro-zoo preference for proto-zoo	*namelist.trc.sms*
	rn_gmapoc	macro-zoo preference for POC	*namelist.trc.sms*
	rn_gmaphy	macro-zoo preference for each phyto. type	*namelist.trc.sms*
K^{Z_j}	rn_grkmic	half-saturation constant for	*namelist.trc.sms*
	rn_grkmes	proto-, meso-	*namelist.trc.sms*
	rn_grkmac	and macro-zooplankton	*namelist.trc.sms*
σ^{Z_j}	rn_sigmic	Fraction of zooplankton	*namelist.trc.sms*
	rn_sigmes	excretion as DIC	
	rn_sigmac		
ξ^{Z_j}	rn_unamic	Fraction of unassimilated	*namelist.trc.sms*
	rn_unames	food by proto-, meso-	
	rn_unamac	and macro-zooplankton	
MGE_{Z_j}	micrge	model growth of efficiency	*bgcbio.F90*
	mesoge	of proto-, meso- and	
	macrge	macro-zooplankton	
$R_{0^\circ}^{Z_j}$	rn_resmic	Respiration at 0°C of	*namelist.trc.sms*
	rn_resmes	proto-, meso-	*namelist.trc.sms*
	rn_resmac	and macro-zooplankton	*namelist.trc.sms*
d_{Z_j}	rn_retmic	Temperature dependence of resipration of	*namelist.trc.sms*
	rn_retmes	proto-, meso-	*namelist.trc.sms*
	rn_retmac	and macro-zooplankton	*namelist.trc.sms*
$m_{0^\circ}^Z$	rn_mormes	mortality at 0°C of meso-zoo.	*namelist.trc.sms*
	rn_mormac	and macro-zooplankton	*namelist.trc.sms*
c_{Z_j}	rn_motmes	temperature dependence of mortality	*namelist.trc.sms*
	rn_motmac	for meso and macro-zooplankton	*namelist.trc.sms*
GGE_{Z_j}	rn_ggemic	Growth efficiency	*namelist.trc.sms*
	rn_ggemes	of proto-, meso- and	*namelist.trc.sms*
	rn_ggemac	macro-zooplankton	*namelist.trc.sms*

$$\lambda^*_{OC}(T) = M_{0^\circ} * b^T_{BAC} \frac{\eta_O * \sum_k p^{BAC}_{F_k} F_k}{K^{BAC}_{DOC} + \sum_k p^{BAC}_{F_k} F_k}, \tag{18}$$

where M_{0° is the maximum mineralisation rate at 0° C, b_{BAC} is the temperature dependence of the mineralisation rate ($b^{10} = Q_{10}$) and T is the local seawater temperature in °Celsius. Each food source is associated with a preference p^{BAC}_F. $K_{DOC}BAC$ is the half-saturation constant for mineralisation of DOC. Bacterial growth is dependent on the available oxygen: $\eta_O = \frac{OXY+3*10^{-6}}{OXY+10*10^{-6}}$, which leads to a maximum bacterial growth rate in the absence of oxygen that is 0.3 times the maximum growth rate at high oxygen.

$R^{BAC}_{0^\circ}$ is the respiration rate at 0°C, d_{BAC} is the temperature dependence of the respiration ($d^{10} = Q_{10}$).

Bacterial growth efficiency BGE, which describes the fraction of mineralised food incorporated into bacterial biomass, is a function temperature and iron availability :

$$BGE = \frac{min(BGE_{0^\circ} - e * T, FER_{BAC} + \lambda^*_{POC} Fe + \lambda^*_{GOC} Fe)}{max((\lambda^*_{DOC} DOC + \lambda^*_{POC} POC + \lambda^*_{GOC} GOC) * Fe/C, 1e-25)} \tag{19}$$

where BGE_{0° is the bacterial growth efficiency at 0° and e is the temperature dependence of bacteria growth, FER_{BAC} is the uptake of dissolved Fe (see equation 47)and $\lambda^*_{GOC}, \lambda^*_{DOC}, \lambda^*_{POC}$ are the remineralisation rates for DOC, GOC and POC respectively as defined above. The remineralisation of iron in POC and GOC is given by:

$$\lambda^*_{POC} Fe = M_{0^\circ} * b^T_{BAC} \frac{\eta_O * \sum_k p^{BAC}_{F_k} SFE}{K^{BAC}_{DOC} + \sum_k p^{BAC}_{F_k} F_k} \tag{20}$$

and

$$\lambda^*_{GOC} Fe = M_{0^\circ} * b^T_{BAC} \frac{\eta_O * \sum_k p^{BAC}_{F_k} BFE}{K^{BAC}_{DOC} + \sum_k p^{BAC}_{F_k} F_k} \tag{21}$$

Grazing of bacteria by zooplankton is described in the previous section.

Table 6: List of parameters and variables used to calculate the evolution of pico-heterotrophs

Term	**Variable**	**Description**	**Defined in**
M_{0°	rn_grabac	Maximum growth rate for bacteria	*namelist.trc.sms*
K^{BAC}_{DOC}	rn_kmobac	DOC half saturation constant of bacteria	*namelist.trc.sms*
p^{BAC}_F	rn_gbadoc	bacterial preference for DOC	*namelist.trc.sms*
	rn_gbapoc	bacterial preference for POC	*namelist.trc.sms*
	rn_gbagoc	bacterial preference for GOC	*namelist.trc.sms*
BGE_{0°	rn_ggebac	Bacterial growth efficiency at 0°	*namelist.trc.sms*
$R^{BAC}_{0^\circ}$	rn_resbac	respiration at 0°C	*namelist.trc.sms*
d_{BAC}	rn_retbac	Temperature dependence of respiration	*namelist.trc.sms*
e	rn_ggtbac	Temperature dependence of bacterial growth efficiency	*namelist.trc.sms*
FER_{BAC}	ubafer	Uptake of dissolved Fe by bacteria	*bgcsnk.F90*
η_O	$\frac{OXY+3*10^{-6}}{OXY+10*10^{-6}}$	oxygen limitation to bacteria growth	
$\lambda^*_{POC} Fe$	ofer	remineralisation of Fe in POC	*bgcsnk.F90*
$\lambda^*_{GOC} Fe$	ofer2	remineralisation of Fe in GOC	*bgcsnk.F90*
$\lambda^\star_{DOC} DOC$	olimi	remineralisation of DOC	*bgcnul.F90 ,bgcsnk.F90*
$\lambda^\star_{POC} POC$	orem	remineralisation of POC	*bgcnul.F90 ,bgcsnk.F90*
$\lambda^\star_{GOC} GOC$	orem2	remineralisation of GOC	*bgcnul.F90 ,bgcsnk.F90*

3.2.1 Denitrification

When waters become suboxic, bacteria can also use nitrate in order to gain oxidative power for DOC remineralization. Hence, there is a (bacterial) denitrification term in the model.

4 Organic matter and bacterial remineralisation

The source and sinks for dissolved organic carbon (DOC) and small (POC) and large (GOC) particulate carbon are shown in Figure 4

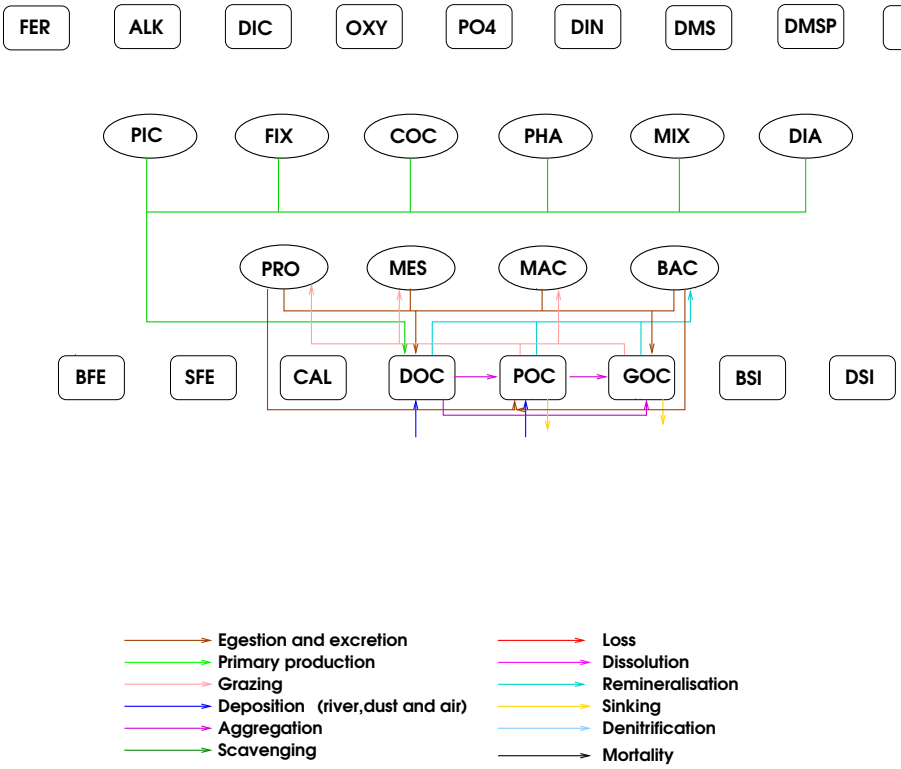

Figure 4: The source and sinks for dissolved organic carbon (DOC) and small (POC) and large (GOC) particulate carbon.

4.1 Dissolved organic carbon - DOC

The evolution of DOC is calculated in the following way:

$$\begin{aligned}\frac{\partial DOC}{\partial t} &= \underbrace{\sum \nu_{P_i}^{tot} \mu^{P_i} P_i}_{production} + \underbrace{\sum_j \left[(1-\sigma^{Z_j})(1-\xi^{Z_j} - MGE^{Z_j}) \sum_k g_{F_k}^{Z_j} * Z_j * F_k \right]}_{egestion} \\ &+ \underbrace{.333 R_{0^\circ}^{BAC} d_{BAC}^T BAC}_{excretion} - \underbrace{\lambda^\star_{DOC} DOC}_{remineralisation} - \underbrace{\Phi_{agg}^{DOC \to POC} - \Phi_{agg}^{DOC \to GOC}}_{aggregation} \\ &+ \underbrace{DOC_{riv}}_{river\ input}, \end{aligned} \tag{22}$$

where $\nu_{P_i}^{tot} = \nu_{P_i} + (1 - L_{lim}^{P_i}) \nu_{P_i}^{max}$ is the fraction of phytoplankton growth which forms DOC. Bacterial degradation of DOC is given by equation 18 for DOC i.e.:

$$\lambda^\star_{DOC} DOC = M_{0^\circ} * b_{BAC}^T \frac{\eta_0 * p_{DOC}^{BAC} * DOC}{K_{DOC}^{BAC} + p_{DOC}^{BAC} DOC}. \tag{23}$$

$\eta_O = \frac{3*10^{-6}+OXY}{OXY+10^{-6}}$ leads to a maximum bacterial growth rate in the absence of oxygen that is 0.3 times the maximum growth rate at high oxygen.

The aggregation functions $\Phi_{agg}^{X \to Y}$ are described in Section 4.2.

Table 7: List of Parameters used in bacterial remineralisation of DOC

Term	Variable	Description	Defined in
ν_{P_i}	rn_docphy	minimum DOC excretion ratio	*namelist.trc.sms*
$\nu_{p_i}^{max}$	rn_domphy	maximum DOC excretion ratio	*namelist.trc.sms*
$g_{F_i}^{Z_j} Z_j$	gramit	Total grazing by	*bgclos.F90*
	gramet	proto,meso and	
	gramat	macro-zooplankton	
d_{BAC}	rn_retbac	temperature dependence of bacterial respiration	*namelist.trc.sms*
$\lambda_{OC}^{\star} OC$	olimi	Remineralisation rate of DOC	
	orem	Remineralisation rate of POC	
	orem2	Remineralisation rate of GOC	*bgcnul.F90* ,*bgcsnk.F90*
K_{PO4}^{BAC}	rn_kmpbac	PO4 half saturation constant	*namelist.trc.sms*
K_{FER}^{BAC}	rn_kmfbac	FER half saturation constant	*namelist.trc.sms*
b_{BAC}	rn_mutpft	temp. dependence of growth rate	*namelist.trc.sms*
DOC_{riv}	depdoc	River input of DOC	*trcini.dgom*

4.2 Particulate aggregation

Particle aggregation through either differential sinking or turbulent coagulation is calculated by:

$$\begin{aligned} \Phi_{agg}^{DOC \to POC} &= \phi_1^{DOC} \epsilon DOC^2 + \phi_2^{DOC} \epsilon DOC\, POC \\ \Phi_{agg}^{DOC \to GOC} &= \phi_3^{DOC} \epsilon\, DOC\, GOC \\ \Phi_{agg}^{POC \to GOC} &= \phi_1^{POC} \epsilon POC^2 + \phi_2^{POC} \epsilon GOC\, POC \\ &\quad + \phi_3^{POC} POC\, GOC + \phi_4^{POC} POC^2 \end{aligned} \tag{24}$$

In which ϵ is the shear rate. The coefficients ϕ were obtained by integrating the standard curvilinear kernels for collisions over the size range of each organic matter pool.

Table 8: List of Parameters used in particulate aggregation

Term	Variable	Description	Defined in
$\Phi_{agg}^{DOC \to POC}$	xaggdoc	DOC-POC aggregation	*bgcsnk.F90*
$\Phi_{agg}^{DOC \to GOC}$	xaggdoc2	DOC-GOC aggregation	*bgcsnk.F90*
$\Phi_{agg}^{POC \to GOC}$	xagg	POC-GOC aggregation	*bgcsnk.F90*
ϕ_1^{DOC}	rn_ag5doc	DOC-POC aggregation	*namelist.trc.sms*
ϕ_2^{DOC}	1000.		
ϕ_3^{DOC}	rn_ag6doc	DOC-GOC aggregation	*namelist.trc.sms*
ϕ_1^{POC}	rn_ag1poc	POC-GOC aggregation	*namelist.trc.sms*
ϕ_2^{POC}	rn_ag2poc	POC-GOC aggregation	*namelist.trc.sms*
ϕ_3^{POC}	rn_ag3poc	POC-GOC aggregation	*namelist.trc.sms*
ϕ_4^{POC}	rn_ag4poc	POC-GOC aggregation	*namelist.trc.sms*

4.3 Sinking

Using the data in Ploug et al. (2008) and applying the drag equations of Buitenhuis et al. (2001) results in a new function describing the relationship between particle density and sinking speed (Buitenhuis et al., 2012):

$$V_{sink} = k_{GOC} * MAX(\rho_{particle} - \rho_{seawater}, \rho_{min})^{S_{GOC}}, \tag{25}$$

where, if ρ_{GOC} (=1.08), ρ_{CAL} (=1.34) and ρ_{DSI} are the densities of the organic matter, $CaCO_3$, and SiO_2 respectively, the particle density $\rho_{particle}$ is calculated by:

$$\rho_{particle} = \frac{(GOC * 240. + CAL * 100. + DSI * 60.)}{\max(\frac{GOC*240.}{\rho_{GOC}} + \frac{CAL*100.}{\rho_{CAL}} + \frac{DSI*60.}{\rho_{DSI}}, 10^{-15})} \tag{26}$$

and

$$\rho_{min} = \left(\frac{S_{POC}}{k_{GOC}}\right)^{S_{GOC}} \tag{27}$$

Table 9: List of Parameters used in sinking

Term	Variable	Description	Defined in
S_{POC}	rn_snkpoc	sinking speed of POC	*namelist.trc.sms*
S_{GOC}	rn_snkgoc	sinking speed parameter for GOC	*namelist.trc.sms*
k_{GOC}	rn_singoc	second sinking speed parameter for GOC	*namelist.trc.sms*
ρ_{min}	dnsmin	density at which GOC sinking speed is rn_snkpoc	*trclsm.dgom.h90*
$\rho_{seawater}$	rhop	density of sea-water	
$\rho_{particle} - \rho_{seawater}$	xdens	density of particle	*bgcsnk.F90*
V_{sink}	xvsink	sinking speed of particle	*bgcsnk.F90*

4.4 Small particulate organic carbon - POC

The temporal evolution of small particulate organic carbon, POC, is calculated as

$$\begin{aligned}\frac{\partial POC}{\partial t} = & \underbrace{\xi^{PRO} * \sum_{F_i} g_{F_i}^{PRO} PRO}_{proto-zooplankton\ unassimilated\ food} - \underbrace{\sum_{Z_j} g_{POC}^{Z_j} * Z_j * POC}_{grazing\ on\ POC} \\ & + \underbrace{0.333 * R_{0^\circ}^{BAC} * d_{BAC}^{T} * BAC}_{excretion} - \underbrace{\lambda_{POC}^{\star} POC}_{POC\ remineralisation} - \underbrace{S_{POC} \frac{\partial POC}{\partial z}}_{POC\ sinking} \\ & + \underbrace{\Phi_{agg}^{DOC \to POC}}_{aggregation\ to\ POC} - \underbrace{\Phi_{agg}^{POC \to GOC}}_{aggregation\ to\ GOC} + \underbrace{POC_{riv}}_{river\ input} .\end{aligned} \tag{28}$$

Here, ξ^{mic} is the unassimilated fraction of grazed material, $g_{F_i}^{mic}$ are the grazing coefficients of proto-zooplankton on food sources F as specified in equation 13, and all others variables are as above.

Table 10: List of parameters and variables used to calculate the evolution of POC

Term	Variable	Description	Defined in
K_{P_i}	rn_mokpft	half saturation constant for mortality	*namelist.trc.sms*
POC_{riv}	deppoc	river input of POC	*trcini.dgom.h*

4.5 Large particulate organic carbon - GOC

The temporal derivative of large particulate organic carbon (GOC) is calculated as

$$\begin{aligned}\frac{\partial GOC}{\partial t} = & \underbrace{\sum_j \xi^{Z_j} \sum_k g_{F_k}^{Z_j} * Z_j * F_k}_{zooplankton\ unassimilated\ food} - \underbrace{\sum_j g_{GOC}^{Z_j} * Z_j * GOC}_{loss\ through\ grazing} + \underbrace{\sum_j m_{0^\circ}^{Z_j} * c^T * Z_j}_{MES,MAC\ mortality} \\ & + \underbrace{\Phi_{agg}^{DOC \to GOC} + \Phi_{agg}^{POC \to GOC} PHA}_{aggregation\ to\ GOC} - \underbrace{\lambda_{GOC}^{\star} GOC}_{GOC remineralisation} - \underbrace{V_{sink} \frac{\partial GOC}{\partial z}}_{GOC sinking} .\end{aligned} \tag{29}$$

ξ^{Z_j} is unassimilated fraction of material grazed by meso- and macro-zooplankton and m^{Z_j} is meso- and macro-zooplankton mortality as in equation (13). V_{sink} is the sinking rate of GOC and is calculated as equation (25).

5 Carbonate chemistry

5.1 Calcite - CAL

Calcification in the model is performed only by phytoplankton calcifiers, COC. Losses of calcifiers result in detached/sinking $CaCO_3$, and enters the tracer CAL. Attached $CaCO_3$ is produced in a fixed ratio to organic matter and therefore there is no tracer for its concentration. It does however reduces alkalinity, ALK, and dissolved inorganic carbon, DIC. The source and sinks for detached carbonate (CAL), dissolved inorganic carbon (DIC) and alkalinity (ALK) are shown in Figure 5

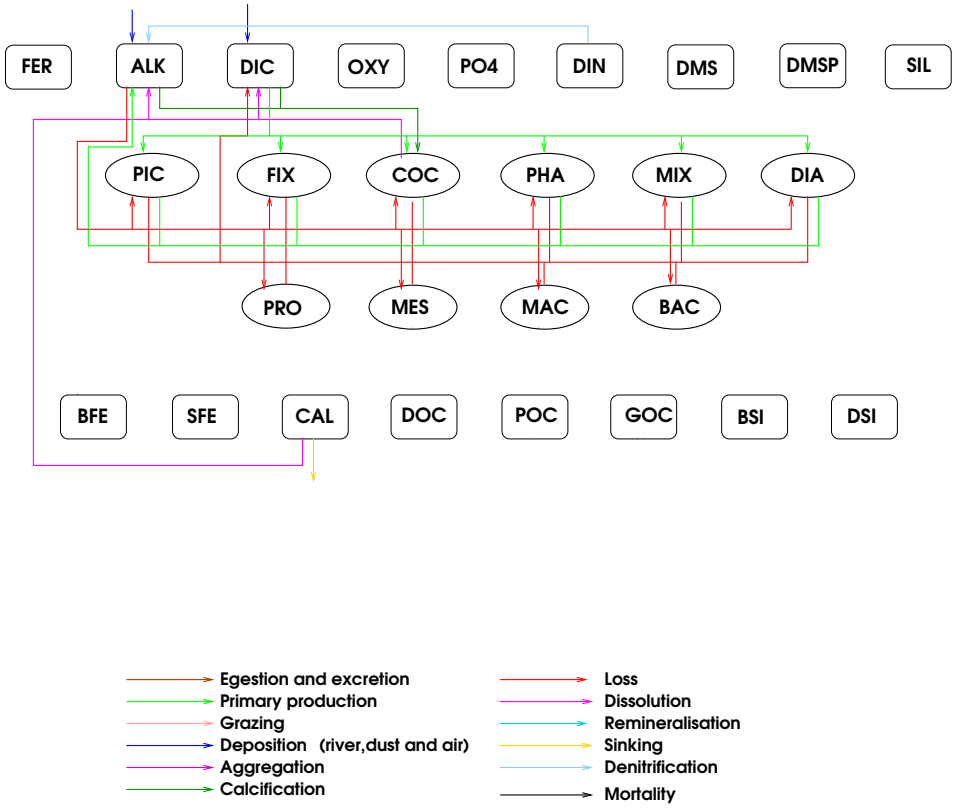

Figure 5: The source and sinks for detached carbonate (CAL), dissolved inorganic carbon (DIC) and alkalinity (ALK).

$$\frac{\partial CaCO_{3attached}}{\partial t} = R_{CAL} \underbrace{\mu^{COC} COC}_{production\ by\ COC} \tag{30}$$

For detached $CaCO_3$, CAL:

$$\frac{\partial CAL}{\partial t} = R_{CAL}(1 - R_{diss}) \left(\underbrace{\mu_0^{COC} \delta_{COC} b_{COC}^T COC}_{COC\ loss} + \underbrace{\sum_j g_{COC}^{Z_j} Z_j * COC}_{grazing\ by\ zooplankton} \right) \tag{31}$$

$$- \underbrace{V_{sink} \frac{\partial CAL}{\partial z}}_{sinking} - \underbrace{\beta_{CO_3} CAL}_{dissolution},$$

where R_{CAL} is the calcification to particulate primary production ratio, R_{diss} is the fraction of attached coccoliths that is dissolved during losses of coccolithophores, V_{sink} is the sinking speed and is described in section 4.3, and β_{CO_3} is the dissolution rate:

$$\beta_{CO_3} = MIN\left(1, \frac{1-\delta_{sat}}{K_{CAL}+\delta_{sat}}\right) \tag{32}$$

where δ_{sat} is the deviation from saturation and K_{CAL} is the half saturation constant for calcite dissolution. β_{CO_3} is 0.25 $month^{-1}$ at the sea surface, and 1 $month^{-1}$ at and below saturation.

CAL is calculated in *bgcbio* and reduced by the fraction dissolved in *bgclys* .

Table 11: List of parameters and variables used to calculate the evolution of calcite

Term	Variable	Description	Defined in
R_{CAL}	rn_coccal	$CaCO_3$ to Carbon ratio	*namelist.trc.sms*
μ^{COC}	prophy	coccolithophorid productivity	*bgcpro.F90*
R_{diss}	rn_discal	Fraction of $CaCO_3$ dissolved during coccolithophorid death	*namelist.trc.sms*
K_{CAL}	rn_lyscal	half saturation constant for calcite dissolution	*namelist.trc.sms*
δ_{sat}	delco3	deviation from saturation	*bgclys.F90*
$\beta_{CO_3}CAL$	remco3	dissolved $CaCO_3$	*bgclys.F90*
$V_{sink}CAL$	sinkcal	sinking speed of $CaCO_3$	*bgcsnk.F90*

5.2 Dissolved inorganic carbon - DIC

The temporal evolution of dissolved inorganic carbon, DIC, is calculated as:

$$\begin{aligned}\frac{\partial DIC}{\partial t} &= \underbrace{-\sum_i \mu^{P_i} * \left(1+\nu_{P_i}^{TOT}\right) P_i}_{primary\ production} + \underbrace{consum}_{consumption} - \underbrace{R_{CAL}\mu^{COC}COC}_{attached\ CaCO_3} \\ &+ R_{diss}R_{CAL}\left(\underbrace{\mu_0^{P_I}\delta_{COC}b_{COC}^T COC}_{COC\ loss} + \underbrace{\sum_j g_{COC}^{Z_j} Z_j COC}_{grazing\ by\ zooplankton}\right) \\ &+ \underbrace{DIC_{riv}}_{river\ input} + \underbrace{\beta_{CO_3}CAL}_{dissolution} + \underbrace{F_{air-sea}^{CO_2}}_{air-sea\ flux}\ .\end{aligned} \tag{33}$$

In addition to the inclusion of grazing by zooplankton remineralistion by bacteria is included as a function of their growth efficiency and respiration (in this case subscript j includes the pico-heterotrophs):

$$\begin{aligned}\text{consum} &= \underbrace{\sum_j \sigma^{Z_j} * (1-\xi^{Z_j} - MGE^{Z_j}) \sum_k g_{F_k}^{Z_j} * Z_j * F_k}_{foodrespiration} \\ &+ \underbrace{(1-BGE) * (\lambda_{DOC}^{\star} DOC + \lambda_{POC}^{\star} POC + \lambda_{GOC}^{\star} GOC)}_{remineralisation} \\ &+ \underbrace{\sum_{j=1}^{3} R_{0^\circ}^{Z_j} d_{Z_j}^T Z_j}_{basal\ respiration} + \underbrace{.333 R_{0^\circ}^{BAC} d_{BAC}^T BAC}_{respiration} + \underbrace{\sum_i \delta_{P_i} b_{P_i}^T \mu_0^{P_i} P_i}_{loss}\ .\end{aligned} \tag{34}$$

The bacterial growth efficiency, BGE, is given by Equation 19. The terms for attached $CaCO_3$ and production of DIC by dissolution are described in Section 5.1. River deposition DIC_{riv} is the input of DIC from rivers, see Section 8.6. The air-to-sea flux is described in section 7.

Dissolved inorganic carbon is calculated in *bgcbio* ; in *bgclys* the $CaCO_3$ dissolution to DIC is included while in *bgcflx* the air-sea flux of DIC is added.

Table 12: List of Parameters used in the evolution of DIC and ALK

Term	Variable	Description	Defined in
BGE	bactge	bacteria growth efficiency	*bgcbio,bgcsnk.F90*
DIC_{riv} $depdic$		river input of DIC	*river.nc*
$R_{\frac{N}{C}}$	alknut	N+S+P to Carbon ratio	*trcini.dgom.F90*
DIC_{riv}	depdic	River deposition of DIC	*trcini.dgom.F90*

5.3 Alkalinity - ALK

The temporal evolution of alkalinity is calculated as:

$$\begin{aligned}\frac{\partial ALK}{\partial t} &= R_{\frac{N}{C}}\Big(\underbrace{\sum_i \mu^{P_i} P_i (1+\nu^{tot}_{P_i})}_{production} - \underbrace{consum}_{consumption}\Big) - \underbrace{2 * R_{CAL}\mu^{coc} COC}_{calcification} \\ &+ \underbrace{2R_{CAL}R_{diss}\big(\mu_0^{COC}\delta_{coc}b^T_{COC}COC + \sum_j g^{Z_j}_{coc} Z_j COC\big)}_{dissolution} \\ &+ \underbrace{DIC_{riv}}_{river\ input} + \underbrace{N_{denit}}_{denitrification} + \underbrace{2 * \beta_{CO_3} CaCO_3}_{dissolution} \end{aligned} \quad (35)$$

where $R_{\frac{N}{C}} = \frac{N+S+P}{C} = \frac{16+6+1}{122}$ is the effect of nutrient uptake and remineralisation on alkalinity (Wolf-Gladrow et al., 2007). The terms for the production of attached $CaCO_3$, dissolved COC and dissolved $CaCO_3$ are described in Section 5.1. River deposition, DIC_{riv} is described in Section 8.6 and denitrification, N_{denit} in Section 6.3.

6 Nutrients and Oxygen

The processes governing the evolution of dissolved iron (FER), large (BFE) and small (SFE) particulate iron, dissolved silica (SIL), biogenic silica (BSI) and detrital silica (DSI) are shown in Figure 6.

The processes governing the evolution of phosphate (PO4), dissolved inorganic nitrogen (DIN) and oxygen (OXY) are shown in Figure 7.

6.1 The Iron Cycle

6.1.1 Fe in PFTs

The iron content of phytoplankton (DFE for silicifiers, NFE for mixed-phytoplankton, CFE for calcifiers, PFE for picophytoplankton, HFE for DMS producers and FFE for N_2-fixers) is given by:

$$\begin{aligned}\frac{\partial Fe^{P_i}}{\partial t} &= \underbrace{\mu_0^{P_i}(1+\delta^{P_i})\rho^{P_i}_{Fe} L^{P_i}_{limFe} b^T_{P_i} P_i}_{production} - \underbrace{\delta_{P_i} * \mu_0^{P_i} * b^T_{P_i} * Fe^{P_i}}_{loss} \\ &- \underbrace{\sum_j g^{Z_j}_{P_i} Z_j * Fe^{P_i}}_{grazing} \end{aligned} \quad (36)$$

$\rho^{P_i}_{Fe}$ describes the iron-light colimitation to phytoplankton growth (Buitenhuis and Geider, 2010) and is given by:

$$\rho^{P_i}_{Fe} = \left(\frac{(Fe_{th}Fe^{max}_{P_i} - Fe^{max}_{P_i})(Fe^{max}_{Pi} - \frac{Fe_{P_i}}{P_i})}{(Fe^{max}_{P_i} - Fe^{min}_{P_i})} + Fe^{max}_{P_i}\right) * L_{light} \quad (37)$$

For phytoplankton other than nitrogen fixers and silicifiers the nutrient limitation is given by:

$$L_{limFe}^{P_i} = \min\left(\frac{PO_4}{PO_4 + K_{PO_4}^{P_i}}, \frac{FER}{FER + K_{FER}^{P_I}}, \frac{DIN}{DIN + K_{DIN}^{P_i}}\right) \tag{38}$$

for silicifiers

$$L_{limFe}^{DIA} = \min\left(\frac{PO_4}{PO_4 + K_{PO_4}^{DIA}}, \frac{FER}{FER + K_{FER}^{DIA}}, \frac{DIN}{DIN + K_{DIN}^{DIA}}, \frac{Si}{Si + K_{Si}^{DIA}}\right). \tag{39}$$

and for nitrogen fixers:

$$L_{limFe}^{FIX} = \min\left(\frac{PO_4}{PO_4 + K_{PO_4}^{FIX}}, \frac{FER}{FER + K_{FER}^{FIX}}, \frac{DIN}{DIN + K_{DIN}^{FIX}} + R_{FIX}\left(1 - \frac{DIN}{DIN + K_{DIN}^{FIX}}\right)\right) \tag{40}$$

The Fe/C ratio of zooplankton is fixed. If zooplankton graze on phytoplankton that have a higher Fe:C ratio than themselves, the excess is remineralised to dissolved iron. If the phytoplankton Fe/C ratio is lower than zooplankton Fe:C, the model growth efficiency (MGE) is decreased:

$$MGE^{Z_j} = MIN\left(1 - \xi^{Z_j}, GGE_{Z_j} + \frac{R_{0^\circ}^{Z_j} d_{Z_j}^T Z_j}{\sum_k g_{F_k}^{Z_j}}, \frac{\sum_k g_{F_k}^{Z_j} \frac{Fe_{F_k}}{F_k}(1 - \xi^{Z_j})}{MAX\left(\sum_k g_{F_k}^{Z_j} \left(\frac{Fe}{C}\right)_Z, 1e-25\right)}\right) \tag{41}$$

6.1.2 Fe in detrital matter - BFE, SFE

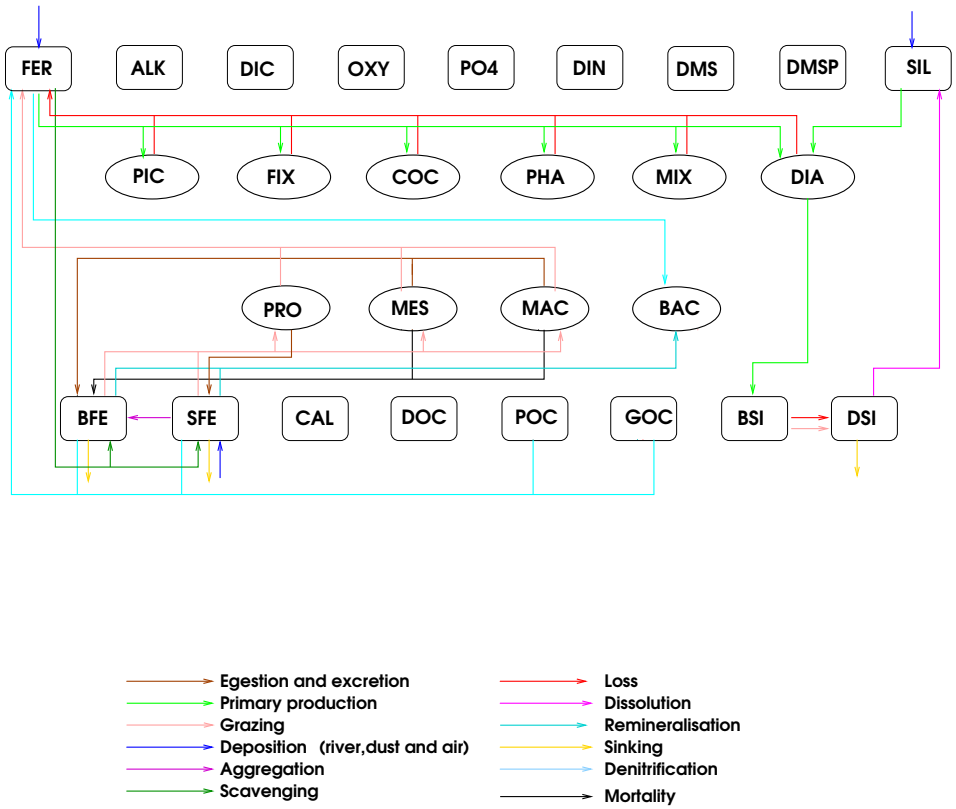

Figure 6: The sources and sinks for dissolved iron (FER), large (BFE) and small (SFE) particulate iron, dissolved silica (SIL), biogenic silica (BSI) and detrital silica (DSI).

Iron in detrital matter is divided into BFE in large organic particles (GOC) and SFE in small organic particles (POC). Production terms of particulate organic iron follow the Fe/C ratio of the source organisms.

There is no iron in DOM, but iron is added from dissolved iron to particulate organic iron during degradation of DOM. Degradation of POM conserves the Fe:C ratio of POM. The bottom correction removes as much carbon from the bottom water layers as is added by rivers (Section 8.6). Because iron is scavenged, the Fe/C ratio of POM sometimes becomes excessive. It is therefore set to a maximum, currently 2^{-6} mol:mol.

$$\begin{aligned}\frac{\partial BFE}{\partial t} &= \underbrace{Fe_{scave}(POC+GOC+DSI+CAL)GOC}_{scavenging} - \underbrace{\sum_j g^{Z_j}_{GOC} * Z_j * GOC\frac{BFE}{GOC}}_{grazing\ loss} \\ &+ \underbrace{\left(\frac{Fe}{C}\right)_Z \sum_{j=MES,MAC} m^{Z_j}_{0^\circ} c^T z^j}_{mortality} + \underbrace{\sum_{j=MES,MAC} \xi^{Z_j} \sum_k g^{Z_j}_{F_k} * Z_j * F_k \frac{Fe_{F_k}}{F_k}}_{unassimilated\ food} \\ &+ \underbrace{\phi^{POC\to GOC}_{agg}\frac{SFE}{POC}}_{Fe\ aggregation} - \underbrace{\lambda^*_{GOC}Fe}_{remineralisation} - \underbrace{V_{sink}\frac{\partial BFE}{\partial z}}_{sinking\ of\ BFE} \end{aligned} \quad (42)$$

$$\begin{aligned}\frac{\partial SFE}{\partial t} &= \underbrace{Fe_{scave} * (POC+GOC+DSI+CAL) * POC}_{scavenging} \\ &- \underbrace{\sum_j g^{Z_j}_{POC} * Z_j * POC\frac{SFE}{POC}}_{grazing\ loss} + \underbrace{\xi^{MIC}\sum_k g^{MIC}_{F_k} * MIC * F_k\frac{Fe_{F_k}}{F_k}}_{unassimilated\ food} \\ &- \underbrace{\phi^{POC\to GOC}_{agg}\frac{SFE}{POC}}_{Fe\ aggregation} - \underbrace{\lambda^*_{POC}Fe}_{remineralisation} - \underbrace{S_{POC}\frac{\partial SFE}{\partial z}}_{sinking\ of\ SFE} + \underbrace{\left(\frac{Fe}{C}\right)_Z POC_{riv}}_{river\ input} \end{aligned} \quad (43)$$

The remineralisation $\lambda^*_{POC}Fe$ is given by equation 18. Fe_{scav} is described below.

6.1.3 Dissolved Fe - FER

The temporal evolution of dissolved iron, FER, is calculated as follows:

$$\begin{aligned}\frac{\partial FER}{\partial t} &= \underbrace{-\mu^{P_i}_0(1+\delta^{P_i})\rho^{P_i}_{Fe}L^{P_i}_{limFe}b^T_{P_i}P_i}_{production} + \underbrace{\delta_{P_i} * \mu^{P_i}_0 * b^T_{P_i} * Fe^{P_i}}_{loss} \\ &+ \underbrace{\sum_j\left(\sum_k g^{z_j}_{f_k} * Z_j * F_k\frac{Fe_{F_k}}{F_k}(1-\xi^{Z_j}) - \left(\frac{Fe}{C}\right)_Z \sum_k g^{Z_j}_{F_k} * Z_j * F_k * MGE^{Z_j}\right)}_{grazing} \\ &+ \underbrace{FER_{remin\_POC\_GOC} + FER_{remin\_BFE\_SFE}}_{mineralisation} - \underbrace{FER_{BAC}}_{bacterial\ demand\ for\ FER} \\ &- \underbrace{Fe_{scav}}_{scavenging} + \underbrace{Fe_{dep}}_{dust\ deposition} + \underbrace{Fe_{riv}}_{river\ input} \end{aligned} \quad (44)$$

Iron is input from rivers, see Section 8.6, and the dissolution of dust from the atmosphere, see Section 8.5. Iron is taken up by phytoplankton during primary production (see above). When iron concentration is above 0.6 nM, it is scavenged by POM: the evolution of scavenged iron, Fe_{scav} is calculated as:

$$\begin{aligned}Fe_{scav} &= k_{scm} + k_{sc} * (POC+GOC+CAL+DSI) * 1e6 \\ &* \frac{-(1+l_{Fe}k_{eq}-FERk_{eq}) + ((1+l_{Fe}k_{eq}-FERk_{eq})^2 + 4FERk_{eq})^{0.5}}{2k_{eq}} \end{aligned} \quad (45)$$

where k_{scm} and k_{sc} are scavenging parameters and k_{eq} is given by:

$$k_{eq} = 10^{17.27-\frac{1565.7}{T-19}}. \quad (46)$$

The iron ligand, l_{Fe} is set to a value of $.6 * 10^-9$ at latitudes North of 30S and below 200m depth, $.3 * 10^-9$ South of 40S and below 200 m, 0 above 100m depth, and linearly interpolated in between. Part of the scavenged iron is added to POM, and part is removed from the model.

Bacteria demand for Fe can be supplied from the remineralisation of BFE and SFE and from dissolved iron. The net effect on FER may be an increase - if remineralisation exceeds the bacterial demand or a decrease if demand exceeds that supplied by remineralisation. Bacterial demand for FER, FER_{BAC} is:

$$FER_{BAC} = \frac{BGE\left(\frac{Fe}{C}\right)_Z * (\lambda^*_{DOC} DOC + \lambda^*_{POC} POC + \lambda^*_{GOC} GOC - \lambda^*_{POC} Fe - \lambda^*_{GOC} Fe)\, FER}{K^{BAC}_{FER} + FER} \tag{47}$$

or zero if this is negative.
The contribution to FER from remineralisation of POC and GOC is:

$$FER_{remin\_POC\_GOC} = \lambda^*_{POC} Fe + \lambda^*_{GOC} Fe \tag{48}$$

The remineralisation of BFE and SFE contributes to FER by:

$$FER_{remin\_BFE\_SFE} = -BGE\left(\frac{Fe}{C}\right)_Z * (\lambda^*_{DOC} DOC + \lambda^*_{POC} POC + \lambda^*_{GOC} GOC - \lambda^*_{POC} Fe - \lambda^*_{GOC} Fe) \tag{49}$$

or zero if this is negative.

Table 13: List of parameters and variables used to calculate the evolution of iron

Term	**Variable**	**Description**	**Defined in**
Fe_{th}	rn_rhfphy	maximum/minimum Fe uptake rate	*namelist.trc.sms*
$FER_{remin\_BFE\_SFE}$	rbafer	Release of dissolved Fe by bacteria	*bgcsnk.F90*
Fe_{scav}	xscave	Iron scavenged by particulate organic matter	*bgcsnk.F90*
Fe_{riv}	depfer	River deposition	*trcini.dgom.F90*
Fe_{dep}	irondep	Dust deposition	*bgcbio.F90*
k_{sc}	rn_scofer	Scavenging rate for iron by particles	*namelist.trc.sms*
k_{scm}	rn_scmfer	Minimum scavenging rate for iron	*namelist.trc.sms*
k_{eq}	xkeq	Scavenging rate parameter	*bgcsnk.F90*
l_{Fe}	ligfer	iron ligand concentration	*bgcsnk.F90*

6.2 The Silicate cycle

Silica is input from rivers and the dissolution of dust from the atmosphere. Growth of diatoms consumes dissolved silica (SIL) from the water to produce hydrated silica (biogenic silica BSI). Loss processes of diatoms produce sinking particulate silica (DSI).

6.2.1 Dissolved SiO_3 - SIL

The temporal evolution of dissolved silica is calculated as:

$$\begin{aligned} \frac{\partial SIL}{\partial t} &= \underbrace{-0.15 \min\left(1, \frac{SIL}{K_{SIL}}\right)\left(\frac{Si}{C}\right)_{DIA} \mu^{DIA} DIA}_{production} + \underbrace{\beta_{Si} DSI}_{dissolution} \\ &+ \underbrace{SIL_{riv}}_{river\ input} + \underbrace{SIL_{dep}}_{dustdeposition} \end{aligned} \tag{50}$$

where $\mu^{DIA} DIA$ is the primary production, in terms of carbon, of diatoms, K_{SIL} is the half saturation constant for SiO_3 in diatoms, β_{Si} is the remineralisation rate of silica which is dependent on temperature,

T and oxygen OXY:

$$\beta_{Si} = \min\left(1.32 * 10^{16} e^{\frac{-11200}{(273.15+T)}}, .1\right) \eta_O. \tag{51}$$

$\left(\frac{Si}{C}\right)_{DIA}$ increases with iron stress and silicate availability:

$$\left(\frac{Si}{C}\right)_{DIA} = 4. - 3 * min\left(\frac{max(0, FER)}{K_{FER}^{DIA}}, 1\right). \tag{52}$$

Observations in the Southern Ocean show a high $\left(\frac{Si}{C}\right)_{DIA}$ ratio in areas with very high Si concentration so $\left(\frac{Si}{C}\right)_{DIA}$ is arbitrarily increased throughout the ocean to reflect this:

$$\left(\frac{Si}{C}\right)_{DIA} = \frac{6. * SIL}{SIL + K_{BSI}}. \tag{53}$$

$\left(\frac{Si}{C}\right)_{DIA}$ is set to the higher of these two ratios.
SIL_{dep} is described in 8.5 and SIL_{riv} in 8.6.

Table 14: List of parameters and variables used to calculate the evolution of silica

Term	Variable	Description	Defined in
β_{Si}	siremin	remineraliation rate of silica	*bgcsnk.F90*
μ_{DIA}	prophy	primary production of diatoms	*bgcpro.F90,bgcnul.F90*
$\frac{Si}{C}_{DIA}$	silfac	Si/C ratio of diatoms	*bgcpro.F90*
K_{FER}^{DIA}	rn_kmfphy	half saturation constant of Fe	*namelist.trc.sms*
K_{BSI}	rn_kmsbsi	half saturation constant for $\left(\frac{Si}{C}\right)$	*namelist.trc.sms*
SIL_{riv}	depsil	river input of SiO_3	*trcini.dgom.F90*
SIL_{atm}	sidep	input of atmospheric silica to the water column	*bgcbio.F90*

6.2.2 Biogenic particulate silica - BSI

The temporal evolution of biogenic silica is calculated as:

$$\begin{aligned} \frac{\partial BSI}{\partial t} &= \underbrace{0.15 \min\left(1, \frac{SIL}{K_{SIL}}\right)\left(\frac{Si}{C}\right)_{DIA} \mu^{DIA} DIA}_{production} \\ &- \underbrace{\sum_j g_{DIA}^{Z_j} * Z_j * DIA \frac{BSI}{DIA}}_{grazing} - \underbrace{\delta_{DIA} \mu_0^{DIA} b^T \frac{BSI}{DIA}}_{loss} \end{aligned} \tag{54}$$

where δ^{DIA} is the excretion ratio for diatoms and $\left(\frac{Si}{C}\right)_{DIA}$ is described above.

6.2.3 Sinking particulate silica - DSI

The temporal evolution of sinking particulate silica is calculated as:

$$\begin{aligned} \frac{\partial DSI}{\partial t} &= \underbrace{\delta_{DIA} \mu_0^{DIA} b^T \frac{BSI}{DIA}}_{loss} - \underbrace{\beta_{Si} DSI}_{dissolution} \\ &+ \underbrace{\sum_j g_{DIA}^{Z_j} * Z_j * DIA \frac{BSI}{DIA}}_{grazing} + \underbrace{V_{sink} \frac{\partial DSI}{\partial z}}_{sinking\ DSI} \end{aligned} \tag{55}$$

where δ^{DIA} is the excretion ratio for diatoms as above.

6.3 Phosphorus and Nitrogen - PO4 and DIN

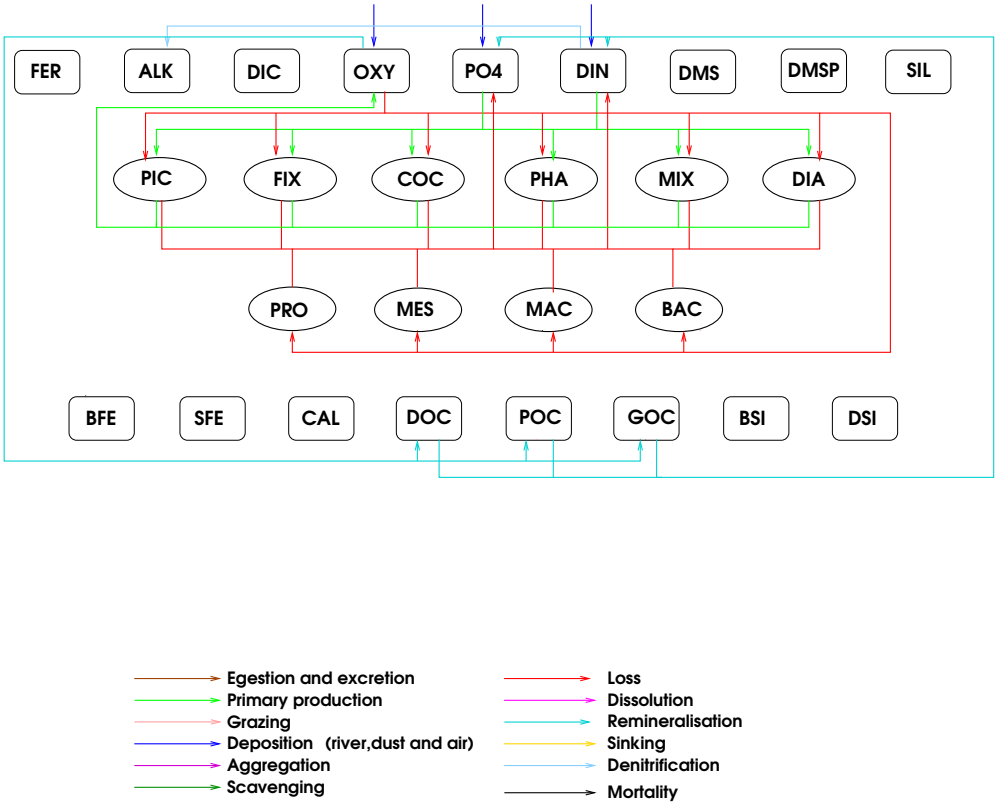

Figure 7: The source and sinks for phophate (PO4), nitrogen (DIN) and oxygen (OXY).

Phosphate is input to the ocean by river deposition; it is consumed during phytoplankton growth and produced during respiration.

$$\frac{\partial PO4}{\partial t} = \underbrace{\sum -\mu^{P_i} P_i \left(1+\nu_{P_i}^{tot}\right)}_{production} + \underbrace{consum}_{consumption} + \underbrace{PO4_{riv}}_{river\ input} \tag{56}$$

$consum$ is defined in equation 34.

Dissolved inorganic nitrogen evolves as:

$$\begin{aligned}\frac{\partial DIN}{\partial t} &= \underbrace{\sum -\mu^{P_i} P_i (1+\nu_{p_i}^{tot}) \frac{N}{C} DIN_{nit}}_{production} + \underbrace{consum * \frac{N}{C}}_{consumption} \\ &- \underbrace{N_{denit}}_{denitrification} + \underbrace{DIN_{riv}\frac{N}{C}}_{river\ input} + \underbrace{DIN_{atm}}_{atmosphere\ deposition}\end{aligned} \tag{57}$$

where

$$N_{denit} = 0.8\left(\frac{O}{C} * consum * resp_{BAC}^{NO_3}\right). \tag{58}$$

$\frac{O}{C} = \frac{172}{122}$ and $resp_{BAC}^{NO_3}$ is the fraction of bacterial respiration that uses NO_3 rather than O_2 and is described in Section 6.4. DIN_{nit} is 1 for all phytoplankton type except for N_2 fixers for which it represents the nitrate limited fraction of growth on NO_3 rather than N_2:

$$DIN_{nit} = \frac{\frac{DIN}{DIN+K^{fix}_{NO_3}}}{\frac{DIN}{DIN+K^{fix}_{NO_3}} + R_{fix}\left(1 - \frac{DIN}{DIN+K^{fix}_{NO_3}}\right)}. \quad (59)$$

Table 15: List of Parameters used in the evolution of phosphate and nitrogen

Term	Variable	Description	Defined in
N_{denit}	denitr	denitrification	*bgcbio.F90*
$PO4_{riv}$	deppo4	River input of phosphate in mole	*trcini.dgom*
DIN_{riv}	depnit	River input of NO_3	*trcini.dgom*
DIN_{atm}	atmdin	Atmosphere input of NO_3	*trcini.dgom*
K^{FIX}_{DIN}	rn_kmnphy	NO_3 half saturation constants for phytoplankton	*namelist.trc.sms*
R_{FIX}	rn_munfix	Fraction of growth rate during N_2 fixation relative to growth on NO_3	*namelist.trc.sms*
DIN_{nit}	dinpft	fraction of phyto growth that is supported by NO_3 rather than N_2	*bgcpro.F90*
$resp^{NO_3}_{BAC}$	nitrfac	fraction of bacterial respiration using NO_3 rather than O_2	*bgcnul.F90*

6.4 Oxygen - OXY

Oxygen is produced during the growth of phytoplankton. It is consumed during the growth of N_2 fixers on N_2 and during the remineralisation described by the term $consum$ in Section 5.2. There is also an exchange of oxygen with the atmosphere.

$$\begin{aligned}\frac{\partial OXY}{\partial t} &= \underbrace{\frac{O}{C}\sum \mu^{P_i} P_i \left(1+\nu^{tot}_{P_i}\right)}_{phytoplankton\ growth} - \underbrace{\frac{N}{C}\mu^{P_{fix}} P_{fix}\left(1+\nu^{tot}_{FIX}\right) 1.25(1-DIN_{nit})}_{growth\ of\ N_2\ fixers\ on N_2} \\ &- \underbrace{\frac{O}{C} consum(1-resp^{NO_3}_{BAC})}_{remineralisation} + \underbrace{F^{O_2}_{air-sea}}_{O_2\ flux\ from\ air\ to\ sea} \end{aligned} \quad (60)$$

The fraction of bacterial respiration that uses NO_3 rather than O_2, $resp^{NO_3}_{BAC}$ is given by:

$$resp^{NO_3}_{BAC} = \frac{\sin\left(\max\left(-.5, \frac{10E-6-OXY}{20E-6+OXY}\right) * \pi\right) + 1}{2} \quad (61)$$

The air-sea exchange of oxygen, $F^{O_2}_{air-sea}$, is given by

$$F^{O_2}_{air-sea} = \left(\frac{O}{N}_{pi} sol_{O_2}\left(1. - e^{20.1050 - 0.0097982 * sstk - 6163.10/sstk}\right) - OXY\right) .3v^2(1-\gamma) \quad (62)$$

The terms are described described in Section 7. It is calculated in ***bgcflx*** .

7 Air-sea exchange of trace gases

The air-sea flux of trace gases (CO_2, O_2, and DMS) is given by the product of gas exchange coefficient and the difference in concentration of the gas across the sea-air interface:

$$F_{air-sea} = k_w * (1-\gamma) * (pC^{air}_{gas} - pC^{sea}_{gas}) \quad (63)$$

where k_w is the gas exchange coefficient, γ is the fraction of the ocean covered by ice, pC_{gas}^{air} is the concentration of the gas in the air directly above the water, and pC_{gas}^{sea} is the sea surface concentration of the gas.

The gas exchange coefficient is calculated according to Wanninkhof (1992) (eq. 3):

$$k_{wannin} = 0.3 * v^2 * \sqrt{660./Schmidt_{gas}} \tag{64}$$

where v is the amplitude of the winds (m/s), sst is the sea surface temperature, and Schmidt$_{gas}$ is the Schmidt number for each gas Wanninkhof (1992).

7.1 CO_2

For the gas exchange coefficient CO_2 Wanninkhof (1992) include a chemical enhancement term:

$$k_{wannin}^{CO_2} = 0.3 * v^2 + 2.5 * (0.5246 + 0.016256 * sst + 0.00049946 * sst^2) \tag{65}$$

For CO_2, $pC_{CO_2}^{air}$ is calculated from the measured mixing ratio of CO_2 in the atmosphere ($C_{CO_2}^{air}$, in ppm) times the solubility of CO_2 in sea water and corrected for 100% water vapor Sarmiento et al. (1992):

$$pC_{CO_2}^{air} = C_{CO_2}^{air} * sol_{CO_2} * (1. - e^{20.1050 - 0.0097982 * sstk - 6163.10/sstk}) \tag{66}$$

where sstk is sea surface temperature in degree Kelvin. The solubility of CO_2 is given by:

$$sol_{CO_2} = e^{c00 + c01/(sstk*.01) + c02*\ln(sstk*.01) + sal*(c03 + c04*qtt + c05*(sstk*.01)^2)} * smicr \tag{67}$$

where sal is the salinity and the coefficents $c00$, $c01$, $c02$, $c03$, $c04$, $c05$ and $smicr$ are given by Wanninkhof (1992). The Schmidt number for CO_2 is given by:

$$Schmidt_{CO_2} = 2073.1 - 125.62 * sst + 3.6276 * sst^2 - 0.043126 * sst^3 \tag{68}$$

$C_{CO_2}^{sea}$ is the concentration of CO_2 in the model, calculated based on the state variables DIC and TALK.

7.2 O_2

For O_2, $pC_{O_2}^{air}$ is calculated from the measured mixing ratio of O_2 in the atmosphere ($C_{O_2}^{air}$, times the solubility of O_2 in seawater, also corrected for 100% water vapor as for CO_2 Sarmiento et al. (1992):

$$pC_{O_2}^{air} = C_{O_2}^{air} * sol_{O_2} * (1. - e^{20.1050 - 0.0097982 * sstk - 6163.10/sstk}) \tag{69}$$

The solubility of O_2 is calculated as follows:

$$\begin{aligned} sol_{O_2} &= e^{ox0 + ox1/(sstk*.01) + ox2*\ln(sstk*.01) + sal*(ox3 + ox4*(sstk*.01) + ox5*(sstk*.01)^2)} \\ &* oxyco \end{aligned} \tag{70}$$

The Schmidt number for O_2 is given by:

$$Schmidt_{O_2} = 1953.4 - 128.0 * sst + 3.9918 * sst^2 - 0.050091 * sst^3 \tag{71}$$

where sal is the salinity and the coefficents $ox0$, $ox1$, $ox2$, $ox3$, $ox4$, $ox5$, and $oxyco$ are given by Wanninkhof (1992).

Table 16: List of parameters and variables used to calculate the evolution of air-sea fluxes

Term	Variable	Description	Defined in
v	wndm	wind speed	
sal	sn (1)	salinity of sea surface layer	
sst	tn (1)	temperature of sea surface (°C)	
$co1$	c00	and other chemical constants	*trcini.dgom.F90*
$Schmidt_{CO_2}$	schmico2	Schmidt number for CO_2	*bgcflx.F90*
$Schmidt_{O_2}$	schmio2	Schmidt number for O_2	*bgcflx.F90*
γ	freeze	fraction of ocean covered by ice	*limflx.F90*
$\frac{O}{N}_{pi}$	atcox	pre-industrial ratio of oxygen to nitrogen	*trcini.dgom.F90*
$F^{O_2}_{air-sea}$	flu16	air-sea oxygen flux	*bgcflx.F90*

8 Model Setup

8.1 Ocean General Circulation Model

The physical model NEMO v3.1 (Madec (2008), http://www.nemo-ocean.eu/About-NEMO/Reference-manuals) was developed by the Laboratoire d' Océanographie Dynamique et de Climatologie (LODYC) to study large scale ocean circulation and its interaction with atmosphere and sea-ice. NEMO is based on the Navier-Stokes equations describing the motions of the fluid and on a non-linear equation of state, which couples the two tracers salinity and temperature to the fluid velocity.

8.2 Sea-Ice Model

NEMO is coupled to the Louvain-La-Neuve Sea-Ice Model (LIM, Timmermann et al., 2005), developed by Fichefet and Morales-Maqueda (1999). LIM has been thoroughly validated for both Arctic and Antarctic conditions, and has been used in a wide range of process studies. Due to the use of an elaborate technique for solving the continuity equations (Prather, 1986), LIM is particularly suited to describing the ice-edge in coarse grid resolutions, which are typically used for climate modelling studies. The physical fields that are advected in LIM are the ice concentration, the snow volume per unit area, the ice volume per unit area, the snow enthalpy per unit area, the ice enthalpy per unit area, and the brine reservoir per unit area. A full model description and details of the coupling to OPA-ORCA can be found in Timmermann et al. (2005).

8.3 Forcing

8.3.1 Physical Forcing

The model is forced by daily wind stress, cloud cover and precipitation from the NCEP/ NCAR reanalysed fields (Kalnay et al., 1996). Sensible and latent heat fluxes are calculated with bulk formulae using the differences between the surface temperature calculated by OPA and the observed air temperature, taking into account local humidity. At the end of each year a water balance is calculated and a uniform water flux correction is applied during the following year to conserve the water mass.

8.4 Initialisation

All model simulations are initialized with observations from the World Ocean Atlas 2009 for temperature (Locarnini et al., 2010), salinity (Antonov et al., 2010) PO_4^{3-},NO_3^-, SiO_3^-, (Garcia et al., 2010b) and O_2 (Garcia et al., 2010a). DIC, alkalinity (GLODAP) observations were from Key et al. (2004). The biological state variables are initialised with the output from previous model runs.

8.5 Dust input

The model is forced with Fe and Si input from monthly dust fluxes taken from Jickells et al. (2005) and interpolated to daily values in *bgcint.F90* . The input is total dust rather than in units of Fe. We assume

0.035g Fe per g of dust and either 8.8g Si per g Fe or, the equivalent, 0.308 g Si per g dust. The solubility of Fe in dust is generally taken to be 2 % and may be set in rn_fersol . The solubility of Si in dust is 7.5 %. Using these values the dust is converted to equivalent Fe, Fe_{dep} and Si, Si_{dep} in units of mol/L/timestep in *bgcbio.F90* .

8.6 River input

Annual fluxes of riverine carbon and nutrient (N, Si, Fe) to the ocean were computed following a global river drainage direction map (DDM30), considering population and basin area (Döll and Lehner, 2002), and river runoff (Kourzoun, 1977; Ludwig and Probst, 1998) at 0.5° increments of latitude and longitude as in da Cunha et al. (2007). This map represents the drainage directions of surface water on all continents, except Antarctica. Cells of the map are connected by their drainage directions and are thus organized into drainage basins. We use the cells corresponding to basin outlets to the ocean as input data for PlankTOM.

Values for DIC_{riv}, DOC_{riv}, POC_{riv}, DIN_{riv}, $PO4_{riv}$, SIL_{riv} and Fe_{riv} as used in the preceding Sections are obtained by multiplying the input by the relevant parameter in Table 17. Thus all riverine inputs may be switched off by setting their parameter to zero.

In order to close the N, Si, and alkalinity cycles of the ocean, as much POM, DOM, SiO2 and CaCO3 is removed from the bottom water layer as is added by rivers and Si in dust.

8.6.1 Dissolved Inorganic Nitrogen (DIN)

To calculate riverine DIN inputs we used a regression model originally developed by Smith et al. (2003):

$$\log DIN = 3.99 + 0.35 \log POP + 0.75 \log R \tag{72}$$

where (DIN) is in mol N km^{-2} y^{-1}, (POP) is population density in people km^{-2}, and (R) is runoff in m y^{-1}. The model describes DIN export by the analysis of 165 systems for which DIN flux data is available (Meybeck and A., 1997), S. Smith and F. Wulff (Eds.), LOICZ-Biogeochemical modelling node, 2000, available at http://data.ecology.su.se/MNODE/]. In this model, riverine DIN export to the coastal zone is a function of basin population density and runoff: On the basis of basin area, basin population (for the year 1990) and runoff provided by the DDM30 map, 16.3 Tg DIN y^{-1} (1.16 Tmol N y^{-1}) are transported to the coastal zone by rivers. In the Smith et al. 2003 model, the average N:P ratio of riverine export is 18:1, which is close to the PISCES-T N:P ratio of 16:1. Nitrogen retention in estuarine areas was not included owing to lack of global data.

8.6.2 Dissolved Silica (Si)

Rivers are responsible for 80% of the inputs of Si to the ocean (Treguer et al., 1995). For an estimate of riverine input of dissolved Si we used the runoff data from the DDM30 map, and applied an average concentration of Si in river waters of 4.2 mg Si/L (Treguer et al., 1995). Si concentration in river water is variable according to basin geology but regional data is not available. Our estimate leads to a dissolved Si river input of 187 Tg Si y^{-1} to the ocean. This value is comparable to the range of 140 $\pm$ 30 Tg Si y^{-1} for a net riverine dissolved Si input to the ocean proposed by Treguer et al. (1995), considering estuarine retention of Si.

8.6.3 Dissolved Iron (Fe)

Rivers and continental shelf sediments supply Fe to surface waters. Because it is extensively removed from the dissolved phase in estuaries, rivers are thought to be a minor source for the open ocean, but not for coastal zones. We used the runoff data from the DDM30 map and applied an average concentration of dissolved Fe in river waters of 40 mg L^{-1} (Martin and Meybeck, 1979; Martin and Whitfield, 1983). As for Si, river basin geology influences Fe concentration in river water, but there is no available global database on riverine Fe. Our estimate leads to a gross dissolved Fe input of 1.75 Tg Fe y^{-1}, comparable to the estimate of 1.45 Tg Fe $^{-1}$ by Chester (1990). During estuarine mixing, flocculation of colloidal Fe and organic matter forms particulate Fe because of the major change in ionic strength upon mixing of fresh water and seawater (de Baar and Jong, 2001). This removal has been well documented in many estuaries. Literature values show that approximately 80 to 99% of the gross dissolved Fe input is lost to the particulate phase in estuaries at low salinities (Boyle et al., 1977; Chester, 1990; Dai and Martin, 1995; Lohan and Bruland,

2006; Sholkovitz, 1978). We apply a removal rate of 99% to our gross Fe flux, and obtained a net input of riverine dissolved Fe to the coastal ocean of 0.02 Tg Fe y^{-1}.

8.6.4 Particulate (POC) and Dissolved Organic (DOC) and Inorganic (DIC) Carbon

The predicted river carbon fluxes are based on models relating river carbon fluxes to their major controlling factors (Ludwig and Probst, 1998; Ludwig, 1996). For POC, sediment flux is the dominant controlling parameter. For DOC, runoff intensity, basin slope, and the amount of soil OC in the basin are the controlling parameters (Ludwig, 1996). We applied this model to the DDM30 data set, and we estimate a gross discharge of 148 Tg C y^{-1} and 189 Tg C y^{-1} for POC and DOC, respectively. We assume that DOC has a conservative behavior in estuaries. These values are in agreement with recent modeled values of 170 Tg C y^{-1} as DOC (Harrison et al., 2005), and 197 Tg C y^{-1} as POC (Beusen et al., 2005; Seitzinger et al., 2005). We used a C:N:P:Fe ratio of 122:16:1:2.44 10^{-4}, thus riverine DOC and POC, when they are remineralized, are also N, P and Fe sources to the ocean. Inorganic carbon is mainly transported by rivers in the dissolved form. For DIC inputs, drainage intensity and river basin lithology are the controlling parameters (Ludwig et al., 1996). We applied this model to the DDM30 data set, and we estimate a DIC and alkalinity discharge of 385 Tg C y^{-1} (32.12 Tmol C y^{-1}).

Table 17: List of Parameters used in river input

Term	Variable	Description	Defined in
	rn_rivdic	river input of DIC	*namelist.trc.sms*
	rn_rivdoc	river input of DOC	*namelist.trc.sms*
	rn_rivfer	river input of Fe	*namelist.trc.sms*
	rn_rivpoc	river input of POC	*namelist.trc.sms*
	rn_rivnit	river input of nitrate	*namelist.trc.sms*
	rn_rivpo4	river input of phosphate	*namelist.trc.sms*
	rn_rivsil	river input of silica	*namelist.trc.sms*
	rn_sedfer	coastal release of Fe	*namelist.trc.sms*

8.7 The namelist.trc.sms file

Values used for the parameters defined in *namelist.trc.sms* are given in the following tables.

Table 18: List of Parameters defined in *namelist.trc.sms*

Parameter	Value	Units	Description
rn_ag1poc	1.2e4	L s (mol d)$^{-1}$ m^{-2}	small POC (POC$_s$ aggregation
rn_ag2poc	1e4	L s (mol d)$^{-1}$ m^{-2}	POC$_s$ - large POC (POC$_l$) aggregation
rn_ag3poc	140	L (mol d)$^{-1}$	POC$_s$ - POC$_l$ aggregation
rn_ag4poc	150	L (mol d)$^{-1}$	POC$_s$ aggregation
rn_ag5doc	180	L s (mol d)$^{-1}$ m^{-2}	DOC - POC$_s$ aggregation
rn_ag6doc	3.9e3	L s (mol d)$^{-1}$ m^{-2}	DOC - POC$_l$ aggregation
rn_alpphy	1.e-6	mol C m^2 (g Chl mol photons)$^{-1}$	initial slope of photsyntheses vs light intensity curve
rn_coccal	0.433	-	ratio of $CaCO_3$ to organic carbon
rn_domphy	0.45	-	maximum DOC excretion ratio for all phyto
rn_discal	0.75	-	fraction of $CaCO_3$ dissolved during coccolithophore mortality
rn_docphy	0.05	-	excretion ratio for all phyto
rn_ekwgrn	0.0232	m^{-1}	green light absorption coefficient of H_2O
rn_ekwred	0.225	m^{-1}	red light absorption coefficient of H_2O
rn_etomax	80.	W m^{-2}	maximum surface insolation
rn_faco18	0.98	-	bacterial fractionation for O_{18}
rn_fersol	0.01	-	solubility of iron in dust
rn_gbadoc	0.088	-	relative preference of BAC grazing for DOC
rn_gbagoc	8.76	-	relative preference of BAC grazing for GOC
rn_gbapoc	8.76	-	relative preference of BAC grazing for POC
rn_ggebac	.21	-	growth efficiency BAC
rn_ggemac	0.3	-	growth efficiency MAC
rn_ggemes	0.25	-	growth efficiency MES
rn_ggemic	0.29	-	growth efficiency PRO
rn_gmabac	0.186	-	relative preference of MAC grazing for BAC
rn_gmagoc	0.186	-	relative preference of MAC grazing for GOC
rn_gmames	1.860	-	relative preference of MAC grazing for MES
rn_gmamic	1.860	-	relative preference of MAC grazing for PRO
rn_gmaphy	1.860	-	relative preference of MAC for DIA
	1.860	-	relative preference of MAC for MIX
	1.860	-	relative preference of MAC for COC
	.930	-	relative preference of MAC for PIC
	1.860	-	relative preference of MAC for PHA
	.186	-	relative preference of MAC for FIX
rn_gmapoc	0.186	-	relative preference of MES grazing for POC
rn_gmebac	.165	-	relative preference of MES grazing for BAC
rn_gmegoc	0.165	-	relative preference of MES grazing for GOC
rn_gmemic	3.302	-	relative preference of MES grazing for PRO
rn_gmephy	1.651	-	relative preference of MES for DIA
	1.238	-	relative preference of MES for MIX
	1.238	-	relative preference of MES for COC
	1.238	-	relative preference of MES for PIC
	1.238	-	relative preference of MES for PHA
	0.165	-	relative preference of MES for FIX
rn_gmepoc	0.165	-	relative preference of MES grazing for POC
rn_gmibac	2.480	-	relative preference of PRO grazing for BAC
rn_gmigoc	0.062	-	relative preference of PRO grazing for GOC
rn_gmiphy	0.620	-	relative preference of MIC for DIA
	1.240	-	relative preference of MIC for MIX

Continued on next page

Table 18 – continued from previous page

Parameter	Value	Units	Description
	1.240	-	relative preference of MIC for COC
	1.240	-	relative preference of MIC for PIC
	1.240	-	relative preference of MIC for PHA
	1.240	-	relative preference of MIC for FIX
rn_gmipoc	0.062	-	relative preference of PRO grazing for POC
rn_grabac	3.15	d^{-1}	maximum BAC uptake rate
rn_gramac	0.106	d^{-1}	maximum MAC grazing rate
rn_grames	1.22	d^{-1}	maximum MES grazing rate
rn_gramic	1.59	d^{-1}	maximum PRO grazing rate
rn_grkmac	9.e-6	mol L^{-1}	K_m for MAC grazing
rn_grkmes	10.e-6	mol L^{-1}	K_m for MES grazing
rn_grkmic	10.e-6	mol L^{-1}	K_m for PRO grazing
rn_icemac	100.0	%	MAC enhanced recruitment under ice
rn_kgrphy	.0118	L (m g Chl)$^{-1}$	light absorption in blue-green for DIA
	.0257	L (m g Chl)$^{-1}$	light absorption in blue-green for MIX
	.0257	L (m g Chl)$^{-1}$	light absorption in blue-green for COC
	.0696	L (m g Chl)$^{-1}$	light absorption in blue-green for PIC
	.0257	L (m g Chl)$^{-1}$	light absorption in blue-green for PHA
	.0657	L (m g Chl)$^{-1}$	light absorption in blue-green for FIX
rn_kmfbac	0.025e-9	mol L^{-1}	K_m for Fe in DOC remineralisation by bacteria
rn_kmfphy	40.e-9	mol L^{-1}	K_m^{Fe} for DIA
	25.e-9	mol L^{-1}	K_m^{Fe} for MIX
	25.e-9	mol L^{-1}	K_m^{Fe} for COC
	10.e-9	mol L^{-1}	K_m^{Fe} for PIC
	25.e-9	mol L^{-1}	K_m^{Fe} for PHA
	40.e-9	mol L^{-1}	K_m^{Fe} for FIX
rn_kmnphy	2.e-6	mol L^{-1}	K_m^{N} for DIA
	2.0e-6	mol L^{-1}	K_m^{N} for MIX
	2.0e-6	mol L^{-1}	K_m^{N} for COC
	2.0e-6	mol L^{-1}	K_m^{N} for DIA
	3.0e-6	mol L^{-1}	K_m^{N} for MIX
	13.0e-6	mol L^{-1}	K_m^{N} for COC
rn_kmobac	1e-7	mol L^{-1}	K_m for DOC in DOC remineralisation by bacteria
rn_kmpbac	1e-7	mol L^{-1}	K_m for PO_4
rn_kmpphy	7.6e-6	mol L^{-1}	$K_m^{PO_4}$ for DIA
	12.2e-6	mol L^{-1}	$K_m^{PO_4}$ for MIX
	15.9e-6	mol L^{-1}	$K_m^{PO_4}$ for COC
	15.9e-6	mol L^{-1}	$K_m^{PO_4}$ for PIC
	97.6e-6	mol L^{-1}	$K_m^{PO_4}$ for PHA
	24.4e-6	mol L^{-1}	$K_m^{PO_4}$ for FIX
rn_kmsbsi	20e-6	mol L^{-1}	K_m for the Si/C ratio of DIA
rn_krdphy	.0056	L (m g Chl)$^{-1}$	light absorption in red for DIA
	.0098	L (m g Chl)$^{-1}$	light absorption in red for MIX
	.0098	L (m g Chl)$^{-1}$	light absorption in red for COC
	.0197	L (m g Chl)$^{-1}$	light absorption in red for PIC
	.0098	L (m g Chl)$^{-1}$	light absorption in red for PHA
	.0181	L (m g Chl)$^{-1}$	light absorption in red for FIX
rn_lyscal	10e-5	mol L^{-1}	inertia conc. for $CaCO_3$ dissolution
rn_mormac	0.020	d^{-1}	MAC mortality rate
rn_mormes	0.040	d^{-1}	MES mortality rate
rn_motmac	1.0481	-	temp. dependence of MAC mortality
rn_motmes	1.1161	-	temp. dependence of MES mortality
rn_mumpft	0.44	d^{-1}	maximum growth rate DIA
	0.35	d^{-1}	maximum growth rate MIX

Continued on next page

Table 18 – continued from previous page

Parameter	Value	Units	Description
	0.70	d^{-1}	maximum growth rate COC
	0.26	d^{-1}	maximum growth rate PIC
	0.68	d^{-1}	maximum growth rate PHA
	0.046	d^{-1}	maximum growth rate FIX
rn_munfix	0.56	-	Fraction of growth rate during N2fix relative to growth on NO3
rn_mutpft	1.0400	-	temp. dependence of proto-zooplankton
	1.0242	-	temp. dependence of meso-zooplankton
	1.1165	-	temp. dependence of macro-zooplankton
	1.0680	-	temp. dependence of DIA
	1.0461	-	temp. dependence of MIX
	1.0132	-	temp. dependence of COC
	1.0611	-	temp. dependence of PIC
	1.0520	-	temp. dependence of PHA
	1.0623	-	temp. dependence of FIX
	1.0379	-	temp. dependence of BAC
rn_qmaphy	2.e-7	-	maximum quota for Fe for all phyto
rn_qmiphy	4.0e-6	-	minimum quota for Fe for all phyto
rn_qopphy	8.6e-6	-	optimal quota for Fe for all phyto
rn_resbac	0.10	d^{-1}	BAC respiration at 0°C
rn_resmac	0.018	d^{-1}	MAC respiration at 0°C
rn_resmes	0.028	d^{-1}	MES respiration at 0°C
rn_resmic	0.010	d^{-1}	PRO respiration at 0°C
rn_resphy	0.012	-	fractional phytoplankton loss rate: DIA
	0.15	-	fractional phytoplankton loss rate: MIX
	0.15	-	fractional phytoplankton loss rate: COC
	0.15	-	fractional phytoplankton loss rate: PIC
	0.15	-	fractional phytoplankton loss rate: PHA
	0.15	-	fractional phytoplankton loss rate: FIX
rn_retbac	1.0494	-	temp. dependence of BAC respiration
rn_retmac	1.0942	-	temp. dependence of MAC respiration
rn_retmes	1.0887	-	temp. dependence of MES respiration
rn_retmic	1.0897	-	temp. dependence of PRO respiration
rn_rhfphy	29.	-	maximum/minimum Fe uptake rate
rn_rivdic	1.	-	(1 - estuarine retention fraction) of river DIC
rn_rivdoc	1.	-	(1 - estuarine retention fraction) of river DOC
rn_rivpoc	0.55	-	(1 - estuarine retention fraction) of river POC
rn_rivpo4	1.	-	(1 - estuarine retention fraction) of river PO_4
rn_rivsil	1.	-	(1 - estuarine retention fraction) of river SIL
rn_rivfer	0.25	-	(1 - estuarine retention fraction) of river FER
rn_scofer	1.e-3	$(\text{mol L}^{-1})^{-0.6}\ \text{d}^{-1}$	scavenging of Fe
rn_scmfer	1.e-3	$(\text{mol L}^{-1})^{-0.6}\ \text{d}^{-1}$	minimum scavenging of Fe
rn_sedfer	1e-11	mol L^{-1}	coastal release of Fe
rn_sigmac	0.70	-	fraction of MAC excretion as PO_4
rn_sigmes	0.68	-	fraction of MES excretion as PO_4
rn_sigmic	0.66	-	fraction of PRO excretion as DOM
rn_sildia	.42e-6	mol L^{-1}	$K_m^{SiO_3}$ for diatoms
rn_singoc	.0303	$\text{m}^2\ (\text{kg d})^{-1}$	Sinking rate parameter of POC_l, $CaCO_3$ and DSi
rn_snkgoc	.6923	-	sinking rate parameter of POC_l,$CaCO_3$ and SiO_2
rn_snkpoc	3.0	m d^{-1}	sinking speed of POC_s
rn_thmphy	.7	g mol^{-1}	maximum CHL:C ratio for DIA
	.4	g mol^{-1}	maximum CHL:C ratio for MIX
	.4	g mol^{-1}	maximum CHL:C ratio for COC
	.4	g mol^{-1}	maximum CHL:C ratio for PIC
	.5	g mol^{-1}	maximum CHL:C ratio for PHA

Continued on next page

Table 18 – continued from previous page

Parameter	Value	Units	Description
	.3	g mol^{-1}	maximum CHL:C ratio for FIX
rn_unamac	0.18	-	unassimilated fraction of phyto during MAC grazing
rn_unames	0.3	-	unassimilated fraction of phyto during MES grazing
rn_unamic	0.13	-	unassimilated fraction of phyto during PRO grazing

References

Antonov, J. I., Seidov, D., Boyer, T., Locarnini, R., Mishonov, A., Garcia, H., Baranova, O., Zweng, M., and Johnson, D. (2010). *World Ocean Atlas 2009, Volume 2: Salinity.* S. Levitus, Ed. NOAA Atlas NESDIS 69, U.S. Government Printing Office, Washington, D.C.

Beusen, A., Dekkers, A., Bouwman, A., Ludwig, W., and Harrison, J. (2005). Estimation of global river transport of sediments and associated particulate C, N, and P. *Global Biogeochemical Cycles*, 19(4).

Boyle, E., Edmond, J., and Sholkovitz, E. (1977). Mechanism of iron removal in estuaries. *Geochimica et Cosmochimica Acta*, 41(9):1313–1324.

Buitenhuis, E., Hashioka, T., and Quéré, L. (2012). Combined constraints on ocean primary production and phytoplankton biomass from observations and a model. *in prep.*

Buitenhuis, E., Le Quere, C., Aumont, O., Beaugrand, G., Bunker, A., Hirst, A., Ikeda, T., O'Brien, T., Piontkovski, S., and Straile, D. (2006). Biogeochemical fluxes through mesozooplankton. *Global Biogeochemical Cycles*, 20:GB2003, doi:10.1029/2005GB002511.

Buitenhuis, E., van der Wal, P., and de Baar, H. J. (2001). Blooms of emiliana huxleyi are sinks of atmospheric carbon dioxide: a field and mesocosm study derived simulation. *Global Biogeochemical Cycles*, 15:577–587.

Buitenhuis, E. T. and Geider, R. (2010). A model of phytoplankton acclimation to iron-light colimitation. *Limnol. Oceanogr*, 55(2):714–724.

Chester, R. (1990). *Marine Geochemistry*. Unwin Hyman.

da Cunha, L., Buitenhuis, E. T., Le Quéré, C., Giraud, X., and Ludwig, W. (2007). Potential impact of changes in river nutrient supply on global ocean biogeochemistry. *Global Biogeochemical Cycles*, 21:GB4007, doi:10.1029/2006GB002718.

Dai, M. and Martin, J. (1995). First data on trace-metal level and behavior in 2 major arctic river-estuarine systems (ob and yenisey) and in the adjacent kara sea, russia. *Earth And Planetary Science Letters*, 131(3-4):127–141.

de Baar, H. J. W. and Jong, J. T. M. D. (2001). Distributions, sources and sinks of iron in seawater. In Turner, D. R. and Hunter, K. A., editors, *The Biogeochemistry of Iron in Seawater*, pages 123–153. John Wiley.

Döll, P. and Lehner, B. (2002). Validation of a new global 30-min drainage direction map. *Journal Of Hydrology*, 258(1-4):214–231.

Fichefet, T. and Morales-Maqueda, M. A. (1999). Modelling the influence of snow accumulation and snow-ice formation on the seasonal cycle of the Antarctic sea-ice cover. *Climate Dynamics*, 15(4):251–268.

Garcia, H. E., Locarnini, R., Boyer, T., Antonov, J., Baranova, O., Zweng, M., , and Johnson, D. (2010a). *World Ocean Atlas 2009, Volume 3: Dissolved Oxygen, Apparent Oxygen Utilization, and Oxygen Saturation.* S. Levitus, Ed. NOAA Atlas NESDIS 70, U.S. Government Printing Office, Washington, D.C.

Garcia, H. E., Locarnini, R., Boyer, T., Antonov, J., Zweng, M., Baranova, O., and Johnson, D. (2010b). *World Ocean Atlas 2009, Volume 4: Nutrients (phosphate, nitrate, silicate).* S. Levitus, Ed. NOAA Atlas NESDIS 71, U.S. Government Printing Office, Washington, D.C.

Harrison, J., Caraco, N., and Seitzinger, S. (2005). Global patterns and sources of dissolved organic matter export to the coastal zone: Results from a spatially explicit, global model. *Global Biogeochemical Cycles*, 19(4).

Jickells, T. D., An, Z. S., Andersen, K. K., Baker, A. R., Bergametti, G., Brooks, N., Cao, J. J., Boyd, P. W., Duce, R. A., Hunter, K. A., Kawahata, H., Kubilay, N., laRoche, J., Liss, P., Mahowald, N., Prospero, J. M., Ridgwell, A. J., Tegen, I., and Torres, R. (2005). Global iron connections betwen desert dust, ocean biogechemistry, and climate. *Science*, 308:67–71.

Kalnay, E., Kanamitsu, M., Kistler, R., Collins, W., Deaven, D., Gandin, L., Iredell, M., Saha, S., White, G., Woollen, J., Zhu, Y., Chelliah, M., Ebisuzaki, W., Higgins, W., Janowiak, J., Mo, K. C., Ropelewski, C., Wang, J., Leetmaa, A., Reynolds, R., Jenne, R., and Joseph, D. (1996). The NCEP/NCAR 40-year reanalysis project. *Bulletin of the American Meteorological Society*, 77(3):437–471.

Key, R., Kozyr, A., Sabine, C., Lee, K., Wanninkhof, R., Bullister, J., Feely, R., Millero, F., Mordy, C., and Peng, T.-H. (2004). A global ocean carbon climatology: Results from glodap. *Global Biogeochemical Cycles*, 18(GB4031).

Kourzoun, V. I. (1977). *Atlas of World Water Balance*. UNESCO.

Locarnini, R. A., Mishonov, A., Antonov, J., Boyer, T., Garcia, H., Baranova, O., Zweng, M., and Johnson, D. (2010). *World Ocean Atlas 2009, Volume 1: Temperature.* S. Levitus, Ed. NOAA Atlas NESDIS 68, U.S. Government Printing Office, Washington, D.C.

Lohan, M. and Bruland, K. (2006). Importance of vertical mixing for additional sources of nitrate and iron to surface waters of the Columbia River plume: Implications for biology. *Marine Chemistry*, 98(2-4):260–273.

Ludwig, W., e. a. (1996). River discharges of carbon to the world's oceans: Determining local inputs of alkalinity and of dissolved and particulate organic carbon. *Comptes Rendus de l'Academie des Sciences - Serie IIA Sci. Terres Planetes*, 323(12):1007–1014.

Ludwig, W., Probst, J., and Kempe, S. (1996). Predicting the oceanic input of organic carbon by continental erosion. *Global Biogeochemical Cycles*, 10(1):23–41.

Ludwig, W. and Probst, J. L. (1998). River sediment discharge to the oceans: Present-day controls and global budgets. *American Journal of Science*, 298:265–295.

Madec, G. (2008). *NEMO ocean engine Note du pole de modélisation*, volume 27. Institut Pierre-Simon Laplace, Paris.

Martin, J.-M. and Meybeck, M. (1979). Elemental mass-balance of material carried by major world rivers. *Marine Chemistry*, 7(3):173–206.

Martin, J.-M. and Whitfield, M. (1983). The significance of the river input of chemical elements to the ocean. In Wong, C., Boyle, E., Bruland, K., and Burton, J.D.and Goldberg, E., editors, *Trace Metals in Sea Water*, pages 265–296. Plenum.

Meybeck, M. and A., R. (1997). River discharges to the oceans: An assessment of suspended solids, major ions, and nutrients. Technical report, U.N. Environ. Programme.

Ploug, H., Iversen, M., Koski, M., and Buitenhuis, E. (2008). Production, oxygen respiration rates and sinking velocity of copepod fecal pellets: Direct measurements of ballasting by opal and calcite. *Limnol. Oceanogr.*, 53:469–476.

Prather, M. C. (1986). Numerical advection by conservation of second-order moments. *Journal of Geophysical Research*, 91(D6):6671–6681.

Sarmiento, J. L., Orr, J. C., and Siegenthaler, U. (1992). A perturbation simulation of CO_2 uptake in an ocean general-circulation model. *Journal of Geophysical Research-Oceans*, 97(C3):3621–3645.

Seitzinger, S., Harrison, J., Dumont, E., Beusen, A., and Bouwman, A. (2005). Sources and delivery of carbon, nitrogen, and phosphorus to the coastal zone: An overview of global nutrient export from watersheds (news) models and their application. *Global Biogeochemical Cycles*, 19(4).

Sholkovitz, E. (1978). Flocculation of dissolved fe, mn, al, cu, ni, co and cd during estuarine mixing. *Earth And Planetary Science Letters*, 41(1):77–86.

Smith, S., Swaney, D., Talaue-McManus, L., Bartley, J., Sandhei, P., McLaughlin, C., Dupra, V., Crossland, C., Buddemeier, R., Maxwell, B., and Wulff, F. (2003). Humans, hydrology, and the distribution of inorganic nutrient loading to the ocean. *Bioscience*, 53(3):235–245.

Timmermann, R., Goosse, H., Madec, G., Fichefet, T., Ethe, C., and Duliere, V. (2005). On the representation of high latitude processes in the ORCA-LIM global coupled sea ice-ocean model. *Ocean Modelling*, 8(1-2):175–201.

Treguer, P., Nelson, D., Vanbennekom, A., Demaster, D., Leynaert, A., and Queguiner, B. (1995). The silica balance in the world ocean - a reestimate. *Science*, 268(5209):375–379.

Wanninkhof, R. (1992). Relationship between wind-speed and gas-exchange over the ocean. *Journal of Geophysical Research-Oceans*, 97(C5):7373–7382.

Wiedenmann, J., Creswell, K., and Mangel, M. (2009). Connecting recruitment of Antarctic krill and sea ice. *Limnol. Oceanogr.*, 54(3):799–811.

Wolf-Gladrow, D. A., Zeebe, R. E., Klaas, C., Koertzinger, A., and Dickson, A. (2007). Total alkalinity: the explicit conservative expression and its application to biogeochmical processes. *Marine chemistry*, 106:287–300.

Index